The feasibility of using decadal changes in the geoelectric field to probe Earth's core

Hisayoshi Shimizu* and Hisashi Utada

Earthquake Research Institute, University of Tokyo
Yayoi 1-1-1, Bunkyo-ku, Tokyo, 113-0032, JAPAN

FAX: +81-3-3812-9417
email: shimizu@eri.u-tokyo.ac.jp

*: Corresponding author

Key words : submarine cable voltage, geoelectric field, Earth's core, kinematic dynamo, toroidal magnetic field

Submitted: July 29, 2003

Revised: December 19, 2003

Abstract

Electric field observations by using 1,000 km scale submarine cables have been performed since early 1990's. One of the main purposes of the observations is to obtain observational constraints on the dynamics of Earth's core such as the strength and the distribution of the toroidal magnetic field and its variation at the core mantle boundary. Several constraints have been obtained until present, but the electromagnetic plausibility of them have not been examined.

In this paper, electromagnetic field variations generated by a simple spherical mean-field kinematic dynamo within an electrically conducting mantle are discussed. The field variations are assumed to be generated by perturbing a steady α^2-dynamo with torsional oscillation type zonal flows having period of 30 years. It is confirmed that the kinematic dynamo can generate the observed amplitude of electric voltage variation ($\sim$ 100mV) naturally. The amplitude of voltage variation is controlled mainly by the energy state of the dynamo, i.e., the magnetic Reynolds numbers, and the strength of the toroidal field variation at the CMB is determined by the magnetic Reynolds numbers and the conductance of the D$''$ layer.

Potential obstacles for the detection of the 100mV signal in 1,000km scale submarine cable voltages are the electric voltages induced by external magnetic field variations (magnetotelluric induction) and that induced by the ocean flow (motional induction). Although the magnetotelluric current with decadal time scales seems negligibly small, the motionally induced electric field variation can be as much as 100mV for 1,000km scale. It is necessary to know the time variation of ocean flux in order to discuss the electric voltages generated in the deep interior of Earth correctly.

1 Introduction

The geomagnetic field has been observed for more than a hundred years (e.g. Langel (1987)). Obtained geomagnetic main field and its variation are often used to study deep interior of Earth such as to find the flow at the surface of the core (e.g. Roberts and Scott (1965)) and to constrain the electrical conductivity of the lower mantle (Alexandrescu et al. (1999)). On the other hand, the geoelectric field has attracted much less attention although it is pointed out that geoelectric field has potential to reveal the dynamics, which cannot be acquired by geomagnetic or other observations, in Earth's interior (e.g. Runcorn (1954, 1964)), probably because only few global scale electric field data were available.

Electric voltage measurements between distant locations more than 1,000km apart have been performed by a joint US-Japan project since early 1990's using long submarine cables retired from telecommunications. The network of the submarine cables for geoelectrical observations in the western Pacific is shown in Fig.1. Although it would be necessary to expand the existing scientific cable network for a better understanding of the global-scale geoelectric field, it is expected that these observations provide additional but unique information to discuss about deep interior of Earth.

One of the main purposes of the global scale electric field observation is to detect the strength and distribution of the toroidal magnetic field and their variation at the core mantle boundary (CMB). Although theoretical estimates of the strength of the toroidal magnetic field in the core considering magnetohydrodynamical balances in a rapidly rotating fluid have been made, the dynamical balances may produce several dynamical

states, and the strength of the toroidal field cannot be determined only by theory at present (see, e.g., Roberts and Glatzmaier (2000)). It is well known that direct observation of the toroidal geomagnetic field is not possible at the surface of Earth. However, the electric current that generates the toroidal field may leak into the mantle from the core because the mantle has small but non-zero electrical conductivity. The electric current should appear at the surface of Earth, in principle (see Runcorn (1954, 1964), Roberts and Lowes (1961)). However, it was concluded by these pioneering workers that the electric field would be too weak to be detected by usual electric field measurements spanning less than 1 km but might be detected only if long cables, such as those shown in Fig.1, are used.

Several attempts to obtain the strength and distribution of the toroidal magnetic field at the CMB using submarine cable voltage data had been made. Lanzerotti et al. (1985) obtained approximate DC value of the electric field from the geoelectric field data of 4 to 85 days long and concluded that the strength of the toroidal field at the CMB is about the same as that of the poloidal field there. However, it is very difficult to obtain the correct DC value because of aliasing: the data length was not long enough compared with the time scale of variation of the geoelectric field of deep internal origin. Moreover, the chemical potential between the electrodes and the surrounding material may be non-zero and it makes estimating the DC values even more difficult. Shimizu et al. (1998) utilized time dependent part of the electric field to avoid the uncertainty involved in using DC values and estimated the amplitude of the decadal variation of the toroidal field at the CMB. It was necessary for them to make some crucial assumptions because the length

of the time series of the submarine cable voltages was about four years, which is not very long. For example, they assumed that the electric field variation is due entirely to thirty-year variation of the geomagnetic main field; one of its signature is the dipole field oscillation of about 50nT (or 0.15%, Yokoyama and Yukutake (1991)). Shimizu et al.(1998) obtained 0.1mV/km as the amplitude of the electric field variation, and found an approximate upper bound of the strength of the toroidal field variation as 1-10 times larger than that of the poloidal field variation at the CMB depending on the mantle conductivity.

Although Shimizu et al. (1998) obtained the observational constraint on the toroidal field variations, it is not known that the constraint is consistent with the physical processes in the core and mantle. In other words, it is not confirmed that the toroidal field variation of the strength at the CMB can be produced by a self-exciting dynamo surrounded by weakly conducting mantle. (Some theoretical discussions on the steady state has been made by Levy and Pearce (1991).)

In this study, electromagnetic field variations generated by a kinematic dynamo surrounded by electrically conducting mantle are calculated in order to test the physical validity of the constraint. The problem is approached in two steps. First, the steady state of the dynamo having conducting mantle is calculated. Then, the steady state is perturbed by applying zonal oscillatory flows in the dynamo region to generate oscillating electromagnetic field. An α^2 dynamo is employed as the steady dynamo because $\alpha\omega$ dynamo, which might be more appropriate as a model for the geodynamo, is very easy to oscillate by itself and change its direction of the magnetic field by the effect of

the dynamo wave (Parker (1955)). The zonal oscillatory flows are chosen to represent the torsional oscillation in the core (Braginsky (1970)), and the period of the oscillation is supposed to be 30 years. The applied oscillatory flows produce electromagnetic field variation of supposed period though the actual causes of the decadal variations are not really certain yet. It turns out that the kinematic dynamo can generate toroidal magnetic field variation at the CMB naturally and the amplitude can be as large as that Shimizu et al.(1998) obtained.

Flows at the core surface have been studied by using the geomagnetic main field and its variation. Jault et al. (1988) showed almost complete angular momentum exchange between the core and mantle for decadal time-scale via possible cylindrical zonal flow using a time series of the flows (see also Jackson et al. (1993) and Bloxham (1998)). However, there is non-uniqueness to determine the core surface flow only by using the geomagnetic field (Backus (1968)) ; physical and/or mathematical hypotheses are necessary to overcome the non-uniqueness. The global electric field at the surface of Earth has a potential to constrain the flow in the Earth's core if it is used with the geomagnetic field. For example, if the electric and magnetic field is known at the CMB, the flow can be determined completely. However, the toroidal field is not known yet and to find correct electric field distribution at the CMB from surface data requires better information on the electric conductivity distribution in the mantle. Nevertheless, some signature of the core flow must be contained in the surface electric field. We will calculate the electric potential distributions due to two zonal oscillatory type flows and examine if they can be distinguished by geoelectric observations using submarine (or other long) cables.

There are two possible sources of geoelectric variations of decadal time-scale other than that due to the geodynamo, and it is not well understood which is dominant in the cable voltages of decadal time-scale. The two possible sources are the magnetotelluric induction in the solid Earth and the motional induction in the ocean. We will estimate the orders of magnitude of global scale voltage induced by the two sources and will examine if it is possible to detect the geodynamo electric field in practice.

Formulation of the kinematic dynamo problem is presented in the next section. The results of the numerical calculations of the α^2-dynamo and perturbed oscillatory dynamo are presented in section 3. The variations of the electric voltage and electric potential distributions are also shown in the section. Detectability of such a signal is discussed in section 4 by quantifying the order of magnitude of the magnetotelluric and motional inductions. Conclusions are given in section 5.

2 Formulation of the kinematic dynamo problem

2.1 Description of the model

The kinematic dynamo model we consider in this paper consists of three regions; the core, where dynamo action operates, the D″layer and the rest of the mantle (see Fig.2). The boundaries of each region are supposed to be spherical, and the electrical conductivities of the regions are constant.

The radius of the core and mantle, r_c and r_a, are set to be 3,500 km and 6,300 km, respectively. The electrical conductivity of the core (σ_C) is supposed as $\sigma_C = 3 \times 10^5$ S/m (Stacey (1992)), and that of the mantle as $\sigma_M = 1$ S/m (see Shankland et al. (1993)).

The outer radius of the D″layer is $r_D = r_c + d$, and the thickness d will be varied in the numerical calculations. The electrical conductivity of the D″layer, σ_D, also will be changed.

The magnetic field generated by self-exciting dynamo must be three dimensional. However, to make the kinematic problem simpler, we are going to take a mean field approach: the large scale magnetic field is assumed to be axisymmetric, and small-scale dynamo process having three dimensionality of magnetic field (and flow) is parameterized by the α-effect (see Moffatt (1978), Krause and Rädler (1980)).

The kinematic dynamo problem is approached in two steps. First, the steady state of the dynamo under the influence of the electrically conducting mantle is obtained. α^2 dynamo is supposed as the steady state for simplicity. The steady state of the α^2 dynamo, magnetic field distribution and critical R_α (see equation (2.1)), are found as an eigenvalue problem.

After the steady state of the α^2 dynamo is obtained, the state is perturbed by applying oscillatory flow. Zonal, axisymmetric torsional oscillation type flows (Braginsky (1970)) having thirty-year period are employed as the oscillating flow. R_α is kept at or a little below the critical value not to produce rapid growth of the magnetic field. By linearity of the induction equation (see equation (3.1)), thirty-year variation of electromagnetic field is expected to be generated by the oscillating flow. The time variation of the magnetic field due to the flow is calculated numerically by integrating the induction equation in time.

2.2 Governing equations in the core

The governing equations in the core ($0 \leq r \leq r_c$) are the mean-field induction equation and continuity equation,

$$\frac{\partial \mathbf{B}}{\partial t} = \nabla \times (\mathbf{v} \times \mathbf{B} + \alpha \mathbf{B}) + \eta_c \nabla^2 \mathbf{B}, \quad \eta_c = \frac{1}{\mu_0 \sigma_C}. \tag{2.1}$$

$$\nabla \cdot \mathbf{B} = 0, \quad \nabla \cdot \mathbf{v} = 0. \tag{2.2}$$

where $\mathbf{B}$ is the magnetic field, $\mathbf{v}$ is the velocity of the flow, $\alpha\mathbf{B}$ represents the α-effect with coefficient α, η_c is the magnetic diffusivity of the core, and μ_0 is the magnetic susceptivity of vacuum.

Because $\mathbf{B}$ and $\mathbf{v}$ are solenoidal, they can be written with poloidal ($\mathbf{B}_P$, $\mathbf{v}_P$) and toroidal ($\mathbf{B}_T$, $\mathbf{v}_T$) vectors as

$$\mathbf{B} = \mathbf{B}_P + \mathbf{B}_T, \quad \mathbf{v} = \mathbf{v}_P + \mathbf{v}_T, \tag{2.3}$$

where, because the field and velocity are assumed axisymmetric,

$$\mathbf{B}_P = \nabla \times \nabla \times (S(r,\theta)\hat{\mathbf{r}}), \mathbf{B}_T = \nabla \times (T(r,\theta)\hat{\mathbf{r}}), \tag{2.4}$$

$$\mathbf{v}_P = U\nabla \times \nabla \times (s(r,\theta)\hat{\mathbf{r}}), \mathbf{v}_T = U\nabla \times (t(r,\theta)\hat{\mathbf{r}}), \tag{2.5}$$

r is radius, θ is colatitude, $\hat{\mathbf{r}}$ is the unit vector in radial direction, and U is a typical size of the velocity.

Usually, the poloidal and toroidal functions are expended with spherical harmonics when equation (2.1) is solved. In this paper, because the problem is axisymmetric, the functions are expanded with Legendre functions $P_n(\theta)$ as

$$S(r,\theta,t) = \sum_n S_n(r,t)P_n(\theta), \quad T(r,\theta,t) = \sum_n T_n(r,t)P_n(\theta), \tag{2.6}$$

$$s(r,\theta,t)=\sum_n s_n(r,t)P_n(\theta),\quad t(r,\theta,t)=\sum_n t_n(r,t)P_j(\theta). \tag{2.7}$$

Note that the α-effect is expanded similarly using Legendre functions. The details of the equations for $S(r,\theta)$ and $T(r,\theta)$ can be found in Roberts and Stix(1972).

2.3 Governing equations in the mantle

The governing equation in the mantle ($r_c < r \leq r_a$) is also the induction equation but without flow;

$$\frac{\partial \mathbf{B}}{\partial t}=-\nabla\times(\eta_X\nabla\times\mathbf{B}),\quad \nabla\cdot\mathbf{B}=0, \tag{2.8}$$

where X is either D (D$''$layer) or M (rest of the mantle), and η_X is the magnetic diffusivity

$$\eta_X=\frac{1}{\mu_0\sigma_X}. \tag{2.9}$$

This equation is general and it is valid when the electrical conductivity has any spatial distributions. However, only the case with constant σ_D and σ_M is considered in this paper to make the problem simpler.

Another simplification can be made if the time-scale separation of the geomagnetic secular variation and the magnetic diffusion time in the mantle is significant. Since the former (decadal) is considered to be much longer than the latter (one year), the electromagnetic field in the mantle, in effect, responds immediately to the forcing field at the CMB to the first order. Therefore, the steady state solution of the electromagnetic field in the mantle may be applied for the problem.

For the steady state, the poloidal magnetic field becomes a potential field in the mantle, which is the same as the poloidal field with insulating mantle. On the other hand, the

toroidal field is different from the non-conducting case. The equation governing $T(r, \theta)$ in the D″layer and the rest of the mantle is written as

$$\sigma_X \frac{\partial}{\partial r}\left(\frac{1}{\sigma_X}\frac{\partial T}{\partial r}\right) + \frac{1}{r^2 \sin\theta}\frac{\partial}{\partial \theta}\left(\sin\theta \frac{\partial T}{\partial \theta}\right) = 0. \tag{2.10}$$

If σ_X is constant, the solution for this problem is written as, after expanding T with Legendre functions (see equation (2.6)),

$$T_n(r) = a_n r^{n+1} + b_n r^{-n}, \tag{2.11}$$

where a_n and b_n are constant (Roberts and Lowes (1961)) which are determined by boundary conditions.

Because the functional form of T (and S) are known in the mantle, we may take the effect of the conducting mantle into account to the core dynamo problem as boundary conditions at the CMB.

2.4 Boundary conditions for the core dynamo problem

It is necessary to consider not only the CMB, but also all the boundaries in the problem to obtain the boundary conditions at the CMB for the dynamo problem. At the boundaries, $r = r_c$, r_D and r_a, the magnetic field, horizontal electric field and radial electric current are continuous. The conditions may be written using the poloidal and toroidal functions S and T as

$$< S >= 0, \quad \left\langle \frac{\partial}{\partial r}\frac{S}{r} \right\rangle = 0, \tag{2.12}$$

$$< T >= 0, \quad \left\langle \frac{1}{\sigma}\frac{\partial T}{\partial r} \right\rangle = 0, \tag{2.13}$$

where $< f >$ indicates the difference of f between the two sides of the boundaries.

It can be confirmed that the poloidal field does not depend on the conductivity distribution if it is potential because the boundary condition for S (equation (2.12)) does not contain the electrical conductivity. Therefore, the boundary condition for S is, at all the boundaries,

$$\frac{dS_n}{dr} + \frac{n}{r} S_n = 0. \tag{2.14}$$

It needs some more considerations to obtain the boundary condition of T at $r = r_c$. By applying (2.13) at $r = r_c$, r_D and r_a, the boundary condition at $r = r_c$ may be written as

$$T_n + \Lambda_n \frac{\partial T_n}{\partial r} = 0, \tag{2.15}$$

where

$$\Lambda_n = -\frac{\sigma_D}{\sigma_C} \frac{[r_c^{n+1}, -r_c^{-n}]\mathbf{A}_n}{[(n+1)r_c^n, nr_c^{-(n+1)}]\mathbf{A}_n} \tag{2.16}$$

and

$$\mathbf{A}_n = \frac{1}{2n+1} \begin{pmatrix} \dfrac{n}{r_a^n}\left(1 - \left(\dfrac{r_a}{r_D}\right)^{2n+1}\right) + \dfrac{\sigma_D}{\sigma_M}\dfrac{1}{r_a^n}\left((n+1) + n\left(\dfrac{r_a}{r_D}\right)^{2n+1}\right) \\ (n+1)r_a^{n+1}\left(1 - \left(\dfrac{r_D}{r_a}\right)^{2n+1}\right) + \dfrac{\sigma_D}{\sigma_M} r_a^{n+1}\left(n + (n+1)\left(\dfrac{r_D}{r_a}\right)^{2n+1}\right) \end{pmatrix}. \tag{2.17}$$

See details of the derivation in Appendix A. Note here that although the boundary condition for T at the surface of the Earth ($r = r_a$) is

$$T_n = 0, \tag{2.18}$$

the radial derivative of T at $r = r_a$ is not necessarily zero: non-zero horizontal electric field due to the toroidal magnetic field appear at the surface of Earth.

2.5 Electric potential at the surface of the Earth

The distribution of the electric potential at the surface of Earth is obtained using the toroidal function in the present case. The electric field in the mantle is entirely due to the toroidal magnetic field because induction effect in the mantle is neglected in this approximation (see equation (2.10)). By Ampere's law,

$$\mathbf{E} = \frac{1}{\mu_0 \sigma} \nabla \times \mathbf{B}, \tag{2.19}$$

so that the electric field at the surface of Earth is written as, considering the axisymmetry,

$$\mathbf{E} = \frac{1}{\mu_0 \sigma_M} \frac{1}{r_c} \frac{\partial^2 T}{\partial \theta \partial r}|_{r=r_a} \hat{\theta}, \tag{2.20}$$

where $\hat{\theta}$ is a unit vector in the θ direction. Only θ component exist in this case and the surface electric potential ($\equiv \psi$), which depends only on θ, can be obtained by integrating the θ component of the electric field by $r d\theta$. Now, we have

$$\psi(\theta, t) = -\int E_\theta r d\theta = -\frac{1}{\sigma_M \mu_0} \frac{\partial T}{\partial r}|_{r=r_a} \ (+\text{const}). \tag{2.21}$$

The r derivative of T at the surface can be obtained directly from the T of equation (2.11) after a_n and b_n are determined by the boundary conditions.

2.6 Non-dimensional equations

Non-dimensionalized equations and boundary conditions will be used in the actual numerical calculations. Let the length scale be r_c, velocity scale be U, magnitude of the α-effect be α_0 and time scale be τ. Induction equation (2.1) may be scaled using the scales above as

$$\frac{R_m}{S_t} \frac{\partial \mathbf{B}}{\partial t} = R_m \nabla \times (\mathbf{v} \times \mathbf{B}) + R_\alpha \nabla \times (\alpha \mathbf{B}) + \nabla^2 \mathbf{B}, \tag{2.22}$$

where R_m is the magnetic Reynolds number, R_α is the α-effect magnetic Reynolds number, S_t is the Strouhal number;

$$R_m = \frac{U r_c}{\eta}, \quad R_\alpha = \frac{\alpha_0 r_c}{\eta}, \quad S_t = \frac{U\tau}{r_c}. \tag{2.23}$$

Note that non-dimensionalized boundary conditions are also employed for the numerical calculations.

2.7 Form of the α effect and zonal oscillatory flows

The α-effect in the core is supposed as (see, e.g. Roberts (1972), Roberts and Stix (1972)),

$$\alpha(r,\theta) = \frac{729}{16} r^8 (1-r^2)^2 \cos\theta. \tag{2.24}$$

This is taken because the form is simple and the magnetic field of dipole symmetry is excited at critical R_α.

2.8 Form of the oscillating zonal shear flow

We employed two flows shown in the following to represent torsional oscillation type flow;

$$\text{Flow 1:} \quad v_\phi = 0.35 * \frac{15}{2} s(1-s^2)(1-r^8)\mathcal{T}(t), \quad \omega = 0.35 * \frac{15}{2}(1-s^2)(1-r^8)\mathcal{T}(t) \tag{2.25}$$

$$\text{Flow 2:} \quad v_\phi = 0.3 * \frac{15}{2} s^3(1-r^8)\mathcal{T}(t), \quad \omega = 0.3 * \frac{15}{2} s^2(1-r^8)\mathcal{T}(t) \tag{2.26}$$

where v_ϕ is the velocity of the ϕ component of the flow, ω is the angular velocity of the flow, $s = r\sin\theta$ is the distance from the Earth's rotation axis, and $\mathcal{T}(t)$ represents time-dependency of the flow. Sinusoidal function of thirty-year period will be assumed for $\mathcal{T}(t)$. Fig.3 shows the angular velocity distributions of the two flows. The angular

velocities within the main body of both flows do not change in the direction of the rotation vector of Earth and the flows becomes zero quickly near the CMB. Both of the flows are normalized such that the maximum of v_ϕ are about 1. In Flow 1, a strong shear exists in the polar region. On the contrary, the equatorial region has a strong shear in Flow 2. Note that the flows can be expressed using only $t_1(r)$ and $t_3(r)$ in the expansion (2.7).

3 Electromagnetic field generated by the kinematic dynamo

Several grid spacings and truncation degrees are tested and $\Delta r = 1/100$ and truncation degree 8 are employed. This particular descretization gives eigenvalue of free decay problem about 0.5 % lower than the analytical value. Some more discussion on the convergence of the numerical calculations is given in Appendix B. (However, the authors recommend readers to read the appendix after they go through section 3.2. The similarity of the results of the oscillatory dynamos obtained using two different sets of grid are employed to examine the convergence.)

Thickness (d) and electrical conductivity (σ_D) of the D″ layer are changed for the calculations to examine the influence of the conductivity (conductance) of the D″ layer on the core dynamo problem. The values of the quantities used in the calculations are summarized in Fig.4.

3.1 Steady α^2-dynamo

$R_m = 0$ is supposed for this problem, i.e., only the α-effect is responsible to generate the magnetic field. Because the problem is linear in magnetic field and α is steady, the

time dependence of the solution is written as

$$\mathbf{B} \propto \mathbf{B}_0 \exp(\lambda t), \tag{3.1}$$

and self exciting dynamo is possible if $\lambda \geq 0$. Now, equation (2.22) becomes

$$\lambda \mathbf{B}_0 = R_\alpha \nabla \times \mathbf{B}_0 + \nabla^2 \mathbf{B}_0. \tag{3.2}$$

It is possible to set $\lambda = 0$ and formulate the problem as an eigenvalue problem for R_α. However, in this paper, we changed R_α and obtained maximum eigenvalue λ for each R_α as has been done by Gubbins (1973). The R_α corresponding to $\lambda = 0$ is found and is called the critical α-effect magnetic Reynolds number ($R_{\alpha cr}$). Note that the eigenfunctions $S_n(r)$ and $T_n(r)$ are normalized such that the maximum value in entire $\{S_n(r), T_n(r)\}$ is 1.

Magnetic field of dipole symmetry is generated at the critical R_α. The first modes for the poloidal and toroidal fields are S_1 and T_2, respectively, and their values at the CMB are larger than other corresponding modes. The eigenfunctions for the two modes with $d = 200$ km and $\sigma_D = 10^2$, 10^4 and 10^5 S/m are shown in Fig.5. It may be seen in the figure that the change of the conductivity of the D″layer has almost no effect on the distribution of S_1. On the other hand, the distribution of T_2 near the CMB is influenced by the conductivity. Especially, the deviation from zero with very high D″conductivity is significant. (Note that $\sigma_D = 10^5$ S/m is too high for the actual D″layer. The result is shown to demonstrate the effect of the mantle conductivity on T_2.)

The sizes of the steady state toroidal and poloidal field at the CMB can be obtained from the eigenfunctions, i.e. $S_n(r)$ and $T_n(r)$ at $R_{\alpha cr}$. Because normalized and non-

dimensional system is used

$$|\mathbf{B}_{P,n}| = |\nabla \times \nabla \times (S_n Y_n(\theta,\phi))| \sim |S_n|, \quad |\mathbf{B}_{T,n}| = |\nabla \times (T_n Y_n(\theta,\phi))| \sim |T_n|. \tag{3.3}$$

Now, let's consider the size of the toroidal field at the CMB. To represent the toroidal field strength, we consider the ratio of T_2 against S_1 at the CMB. See Table 1 for the values of T_2/S_1 at the CMB, and Fig.6 is its plot against the conductance of the D″layer.

It is seen that the ratio is determined by the conductance of the D″layer, and not by the conductivity within it. Also, the toroidal field is much weaker than the poloidal field at the CMB if the conductance is within the range of acceptable values ($\leq O(10^8)$ S).

3.2 Oscillating dynamo by perturbed flow

The steady states found in the previous subsection are perturbed by applying the oscillatory zonal shear flows (see equations (2.25), (2.26) and Fig.3). The period of oscillation is set to 30 years. This period is employed because (i) the observational study by Yokoyama and Yukutake (1991) suggested probable existence of the geomagnetic 30-year variation, and (ii) the torsional oscillation will have period of several tens of years if it exists in the Earth's core. Also, the results find in this model can be compared with the observational constraint obtained by Shimizu et al. (1998).

It is necessary to set the value of R_m/S_t in equation (2.22). It is possible to use r_c to evaluate the size of R_m/S_t. However, because the actual length-scale in which magnetic field changes will be smaller than r_c, especially with the zonal flow, we will take 1000 km as the length-scale for R_m/S_t. Let $\tau = 30$ years and $L = 1000$ km (see equation (2.23)),

then $R_m/S_t = L^2/\eta_c\tau = 1000/3$. This value is used for all the calculations of oscillatory dynamo in this paper.

Typical time-series of the poloidal and toroidal field variations at the CMB generated by flow 2 when $d = 200$ km, σ_D=100 S/m and $R_m = 1000$ are shown in Fig.7. Thirty-year oscillation is generated by the oscillating zonal shear flow. The amplitudes of the oscillations are estimated by using least square fit to the 30 year sinusoidal variation with small linear trend for all the time series we have obtained.

The oscillatory flow produces the ω-effect, and T_2 component is mainly generated by the flow and S_1 component. Therefore, the oscillation amplitude of S_1 and T_2 at the CMB, ΔS_1 and ΔT_2, respectively, are mainly examined.

Fig.8 shows the ratio of the amplitude of the oscillating dipole to the steady dipole, $\Delta S_1/S_1$, at the CMB (and also at the surface of the Earth). It is about 0.05 % if $R_m = 1,000$ and will be about 0.15% if $R_m = 3,000$.

The ratio of ΔT_2 to ΔS_1 when $R_m = 1,000$ is shown in Table 2, and plotted against conductance of the D″layer in Fig.9. The steady α^2 dynamo showed similar dependence, but the ratio is about 10^4 times larger for the perturbed dynamo than for the steady α^2. This is caused by the shear flow that drives electric current in the radial direction and that forces the electric current flow into the D″layer efficiently.

Electric voltage variation between any two locations at the surface of Earth can be calculated using the toroidal field variation in the mantle (see equation (2.21)). By using the snapshot of the electric potential at the surface of the Earth $\psi(\theta, t)$, the voltage

between at locations having colatitudes θ_1 and θ_2 with GND at θ_2 is

$$V(\theta_1, \theta_2, t) = \psi(\theta_1, t) - \psi(\theta_2, t). \tag{3.4}$$

Fig.10 shows the electric voltage variations, which would be measured using some of the cables shown in Fig.1, generated by flow 2 when $d = 200$ km, $\sigma_D = 100$, and R_m=1000. The time series of the voltage are dimensionalized supposing g_1^0=−30,000nT at the surface of Earth. The voltage variation between 55 and 35 degrees of latitude is also shown as a reference. The peak-to-peak amplitudes are 5-15 mV for the cables for this case. The calculated time series of the voltage or Ninomiya-Guam and 55deg-35deg cables show that the amplitude of the variation may be different for the cables having similar extent in north-south direction. This implies that there may be some locations more sensitive to the voltage variations of the geodynamo origin.

The peak-to-peak amplitude of the voltage variations due to the oscillating flow can be estimated by using $\psi(\theta, t)$. Suppose that $V(\theta_1, \theta_2, t)$ takes its maximum and minimum at $t = t_1$ and t_2, respectively. The peak-to-peak amplitude of the voltage variation between θ_1 and θ_2 may be written as

$$\begin{aligned} V(\theta_1, \theta_2, t_1) - V(\theta_1, \theta_2, t_2) &= (\psi(\theta_1, t_1) - \psi(\theta_2, t_1)) - (\psi(\theta_1, t_2) - \psi(\theta_2, t_2)) \\ &= (\psi(\theta_1, t_1) - \psi(\theta_1, t_2)) - (\psi(\theta_2, t_1) - \psi(\theta_2, t_2)) \\ &= \Phi(\theta_1) - \Phi(\theta_2), \end{aligned} \tag{3.5}$$

where we let

$$\Phi(\theta) = \psi(\theta, t_1) - \psi(\theta, t_2). \tag{3.6}$$

Therefore, if we find $\Phi(\theta)$ for each flow and parameter set, we can discuss how much

amplitude of the voltage variation is expected due to the specific flow and parameter set. Note that the sensitivity to the voltage difference at the location is large if $|\partial\Phi(\theta)/\partial\theta|$ is large.

One of the most interesting feature of the electric potential variation might be the difference of the $\Phi(\theta)$ by flow 1 and 2. Distributions of $\Phi(\theta)$ with d = 200km and $R_m = 1000$ are shown in Fig.11. g_1^0=−30,000nT is assumed in this case, too.

Fig.12 shows the σ_D and d dependencies of $\Phi(\theta)$ with flow 2 and $R_m = 1000$. Not very large differences can be seen in the distribution of $\Phi(\theta)$.

R_m dependence of $\Phi(\theta)$ with flow 2 at d = 200 km and σ_D = 100 S/m is shown in Fig.13. As one might expect, $\Phi(\theta)$ is proportional to R_m. The electric voltage amplitude has the information of the flow speed in the core.

3.3 Discussions on the calculated results

It is demonstrated that the steady state toroidal magnetic field produced by the α^2 dynamo is much smaller than the poloidal field at the CMB. On the contrary the toroidal field variation amplitude may be 1-10 times of the poloidal field variation at the CMB. However, it is still not known this is a general feature of dynamo. The oscillating flows employed for the numerical experiment have strong shear near the CMB, and the shear seems efficient to drive electric current, which produces the toroidal magnetic field, into the D″layer and mantle. If a steady-state dynamo has strong radial electric current generation near the CMB, say by strong α-effect or steady shear just below the CMB, the toroidal field at the CMB might be much larger than it is found (up to about 10^{-3} of the poloidal field) in this paper.

The observational constraint on the strength of the toroidal field variation at the CMB obtained by Shimizu et al. (1998), $|\Delta \mathbf{B}_T| \sim 1 - 10 |\Delta \mathbf{B}_P|$ depending on the conductivity (conductance) of the D″layer, is consistent with the present dynamo model, i.e. the toroidal field variations of such strength can be generated naturally under the conditions with physically plausible values of the conductance of the D″-layer (see Fig.9 and Table 2).

It is interesting to see the distribution of $\Phi(\theta)$ is not changed very much due to the conductivity of the D″layer (see Fig.12) but the size of the oscillating toroidal field is changed as in Fig.9. This means that the dynamo produces almost the same amplitude of electric field oscillation at the surface of Earth regardless of the conductance of the D″layer (of course it must be non-zero) if R_α and R_m ($\sim$ energy level of the dynamo) are the same. Therefore, if the state of the dynamo is decided in the core, the electric potential variation at the surface is also decided, but the size of the toroidal magnetic field variation at the CMB may be different due to the conductance of the D″layer.

The amplitudes of dipole magnetic field variation depend linearly on R_m (Figs.8), and R_m=3,000 is required to achieve the dipole field oscillation of $\Delta S_1/S_1$=0.15%. The amplitude of the electric potential variation also depends linearly on R_m, and the perturbed dynamo with $R_m = 3,000$ may produce the electric voltage variation of 50-100 mV for the cables of several thousands km.

The flow speed corresponding to $R_m = 3,000$ is of order 10^{-3}-10^{-2} m/s if L=1,000 $\sim$ 3,000km and η=1$\sim$3 m^2/s. This estimate of flow speed seems too large for the oscillating flow in the Earth's core. However, the relationship between the dipole variation amplitude

and R_m depends strongly on the dynamo model, i.e., the spatial distribution of the steady state magnetic field and that of the zonal oscillating flow, and it is expected to have dynamo models that produces 0.15% of the dipole field oscillation with slower flow speed. (The discussion if such dynamo is suitable for the case of Earth still remains.) Other possibilities are that the decadal variation is not generated entirely by zonal oscillating flow and/or that the observational estimate of amplitude of geomagnetic dipole oscillation made by Yokoyama and Yukutake(1991) is an overestimate.

Fig.11 shows that the distributions of $\Phi(\theta)$ due to the two different flows are significantly different from each other and the distributions may be interpreted considering the shear distribution in the flows. Because flow 1 has strong shear at the polar region and almost no shear in the equatorial region right beneath the CMB, $\Phi(\theta)$ is steep between 40-85 degree in latitude and almost flat between $\pm$30 degree latitude. On the other hand, $\Phi(\theta)$ by flow 2, which has strong shear at the equatorial region just below the CMB, has steep and almost constant gradient throughout 5 to 60 degree latitude, but very small gradient above 60 degree. The difference indicates the possibility to assess the location of strong shear if such large-scale electric potentials are observed at the surface of Earth for a long time. The present distribution of the cable networks (see Fig.1 for the one in the western Pacific) cover lower to middle latitude (up to about 50 degree). It would be informative if we can make geoelectric field observations at higher latitude, though it might be more difficult to analyze such data because of larger disturbances by the external field.

Very simple one dimensional electrical conductivity in the mantle is considered in this study. The conductivity of the D$''$layer has a dominant effect on the toroidal field strength

at the CMB, and the electric and magnetic fields are in the simple form in the kinematic dynamo model because the conductivity in the D″layer assumed constant. It is believed that there is strong heterogeneity in the D″layer, and the non-uniform conductivity will cause mode conversion of the electromagnetic field (see Koyama et al. (2002)). It will be interesting to consider how the dynamo similar to the one employed in this paper behave under non-homogeneous conductivity of the D″layer and how the magnetic and electric field changes due to the inhomogeneity.

4 Submarine cable voltage variations of non-geodynamo origin

It is shown in the previous sections that the submarine cable voltage variations due to the variations of the toroidal field at the CMB may have amplitudes large enough to be detected by using present-day observations. However, there are two other sources of electric field variations which deserve some attention. The one is the electric field variation induced by the geomagnetic external field variations and the other is that generated by the motional induction due to the ocean flow. These variations possibly have decadal time-scales and may have to be separated properly to obtain the geoelectric field variations of the geodynamo origin. We will estimate the order of magnitude of the submarine cable voltage variations by the two sources in this section.

4.1 Induction due to external geomagnetic field variation

The external geomagnetic field variations have various time-scales: daily variation due to the rotation of the Earth, six-month and one-year variation due to the orbital motion

of the Earth, and 11-year variation due to the solar cycle (see e.g., Courtillot and LeMouël (1988)). Although our concern is the decadal time-scale, we will estimate the order of magnitude of the submarine cable voltage variations for all the time-scales listed above.

Faraday's and Ampere's laws may be written as

$$\nabla \times \mathbf{E} = -\frac{\partial \mathbf{B}}{\partial t} = i\omega \mathbf{B}, \tag{4.1}$$

and

$$\frac{1}{\mu_0} \nabla \times \mathbf{B} = \sigma \mathbf{E}. \tag{4.2}$$

Here, $\mathbf{B} \propto \exp(i\omega t)$ is assumed and Ohm's law $\mathbf{j} = \sigma \mathbf{E}$ is used. The electric field induced in vacuum (insulator) may be estimated by using Faraday's law. If the characteristic magnitude of the magnetic field variation is $|\Delta \mathbf{B}|$ and characteristic length-scale of the oscillating magnetic field is L, then the amplitude of induced electric field variation, $|\Delta \mathbf{E}^F|$, may be expressed as

$$|\Delta \mathbf{E}^F| \approx \omega L |\Delta \mathbf{B}|. \tag{4.3}$$

On the other hand, the induced electric field in conducting material may be written with magnetotelluric relationship (e.g. Parkinson and Hutton (1989)) which can be obtained by combining equations (4.1) and (4.2) and can be written as

$$|\Delta \mathbf{E}^{MT}| = \sqrt{\frac{\omega \mu_0}{\sigma_M}} |\Delta \mathbf{B}|. \tag{4.4}$$

Both $|\Delta \mathbf{E}^F|$ and $|\Delta \mathbf{E}^{MT}|$ are estimated and the values of them are shown in Table 3. $\sigma_M = 1$ S/m is employed as in the previous sections. Expected values of the voltage variations measured using 1000km cable, V^F and V^{MT}, are also listed in Table 3.

The daily variation of V^F and V^{MT} are estimated as about 20V and 0.48V, respectively, which is very large compared with that of the geodynamo origin. The daily variation can be seen in actual submarine cable data, and it is one of the main source of variations. Six-month and one-year variations might have the magnitude of voltage variation ($\sim$20-50mV) as large as that of the geodynamo origin. Although they are in comparable magnitude, the time-scales of the variations are known exactly and it is much shorter than the time-scale of our interest. The variations may be filtered out from long time series when the decadal scale variations are discussed. The 11-year variation might not be filtered out from the time-series of electric voltage for decades, but its amplitude is expected to be much smaller than the voltages due to the geodynamo. Therefore, the submarine cable voltages originated from the external magnetic field variations will not cause much trouble for the detection of the decadal geoelectric field variations from the outer core.

4.2 Motional induction due to ocean current

The sea water is a relatively good conductor having electrical conductivity about 3S/m. The ocean current induces electric field during its movements in the geomagnetic field. Submarine cable voltages are sometimes used to monitor ocean flux by using relationships between the fluxes and voltages (e.g. Larsen (1992), Flosadóttir et al. (1997)). The motionally induced voltage variations might mask the electric field variations of the geodynamo origin if the variation of motionally induced voltage has large enough amplitude.

The motionally induced electric field is a potential field if the time variation of the field

and current is not very rapid (e.g. Chave and Luther (1990)). By Ohm's law,

$$\mathbf{j} = \sigma_S(-\nabla\phi + \mathbf{v} \times \mathbf{B}), \tag{4.5}$$

where $\mathbf{j}$ is the electric current density, σ_S is the electric conductivity of the sea water and ϕ is the electric potential ($\mathbf{E} = -\nabla\phi$). By taking divergence of equation (4.5) and applying $\nabla \cdot \mathbf{j} = 0$, the equation governing ϕ is written as

$$\nabla^2\phi = \nabla \cdot (\mathbf{v} \times \mathbf{B}) \tag{4.6}$$

for the ocean having constant electrical conductivity. We may find ϕ by solving equation (4.6) if $\mathbf{v}$, $\mathbf{B}$, and appropriate boundary conditions, which contain the information of the electrical conductivity of the sea-bed, are specified.

Here, we are going to find the distribution of depth average of ϕ ($\equiv \bar{\phi}$) due to model flow of a global-scale gyre in a simplified ocean. Then, we will estimate the order of magnitude of the cable voltage variation due to decadal variation of the geomagnetic field or that of the ocean flow.

The model ocean we consider is a rectangular ocean surrounded by a rigid wall made of electric insulator. The size of the ocean is supposed as 10,000km×6,300km in [East-West]×[North-South], and the depth is assumed to be 4km. Southern edge of the ocean corresponds to the equator. The two-dimensional global circulation model, which can reproduce strong flow at the western boundary of the ocean, by Stommel(1948) is employed as the global-scale gyre (Fig.14). The distribution of the magnetic field is assumed to be of dipole type and the intensity is set as g_1^0=−30,000nT. We consider only the vertical component of the magnetic field in the calculation.

Fig.15 shows the distribution of $\bar{\phi}$ due to the Stommel's flow and axial dipole field. $\bar{\phi}$ is set zero at the western boundary and 3,150km north from the equator(bottom). The asymmetry in the north-south direction is due to the change of the strength of B_z over the area. It is seen that the steady-state motionally-induced voltage can be about 0.3V for a 1,000km cables, and, generally, it will be smaller for longer cables if one end is at or close to the western boundary of the ocean. The steady state electric voltage is large enough to be measured by the present observations.

As mentioned earlier, the motionally induced cable voltages vary with decadal time-scale if the geomagnetic field and/or the ocean current vary with the time-scale.

By (4.6), the electric field is proportional to the magnetic field strength. If the strength of the magnetic field is changed by 0.15%, the contribution due to geomagnetic field variation on the motionally induced voltage is also 0.15%, i.e. as much as 1mV, which is negligibly small compared with the voltage variation of the geodynamo origin.

The decadal variation of the ocean flux is not very well known yet. However, some studies on Kuroshio in the Western Pacific revealed that the amount of decadal variation of the Kuroshio flux is about 30-40% of its steady value (Hibiya, personal communication). By supposing that the flow pattern is approximately the same but the intensity of the flow changes, then the maximum of expected decadal variation of motionally induced voltage will be 0.3V$\times$[30-40%]$\sim$ 0.1V for 1,000km-scale cables. This value is considered as an upper bound of the maximum value because of the physical set-up of the calculation: the medium outside of bottom and side boundary is perfect insulator in the calculation and no leakage currents into the Earth were allowed. The electric potential gradient

is expected to be smaller if non-zero conductivity of the Earth is taken into account. Therefore, amplitude of motionally induced voltages is at most comparable with the voltage variation due to the decadal variation of the geodynamo. This means that the decadal variation of the ocean current should be properly estimated and removed from the cable voltages for the discussion of the electric field originated by the geodynamo. In principle, this can be done because the ocean current can be observed by a lot of other methods.

5 Conclusions

It has been demonstrated using a simple kinematic dynamo model that the torsional oscillation type flows having period of 30 years can generate toroidal field variation as large as or larger than the poloidal field variation at the CMB. The corresponding electric voltages for 1,000km scale at the surface of Earth generated by the kinematic dynamo model is of the same order of magnitude as that Shimizu et al.(1998) obtained observationally in case that the amplitude of dipole oscillation generated by the dynamo is as large as that found by Yokoyama and Yukutake (1991).

The calculated distributions of the electric potential at the surface of Earth due to two torsional oscillation type flows are significantly different. Main features are originated from the locations of strong shear that distorts the poloidal field to generate the toroidal field. It might be possible to constrain the locations if more observations efficiently covering the surface of Earth are made. Global scale electric field observations at higher latitude will be very informative for the purpose.

Some estimate of decadal variation of submarine cable voltages due to non-geodynamo origin is performed. It is unlikely that the cable voltage variations originated from the geodynamo is masked by the magnetotelluric induction due to the external geomagnetic field variations. However, the voltage variation due to the motional induction in the ocean may be as large as that generated by the geodynamo. The motionally induced electric potential variation estimated in this paper is considered to be an upper-bound because no electric current is allowed to leak into the solid Earth from the ocean: the actual variation of the potential is expacted to be smaller. It is desireble to study the motional induction in the ocean with more realistic global ocean current, its time variation, and electric conductivity distribution of the sea bed to understand how large the electric potential variations are. (This may be done using global ocean circulation models.) If it turns out that the potential variations are large, the calculated results should be used to correct the submarine cable voltage data in order to detect the electric signals from the Earth's core. Note that observations using cables laid along the streamline of the ocean current or those laid on the continents can avoid the effect of the motional induction.

Reference

Alexandrescu, M.M., D. Gibert, J.-L. Le Mouël, G. Hulot, and G. Saracco, 1999. An estimate of average lower mantle conductivity by wavelet analysis of geomagnetic jerks. J. Geophys. Res., 104(B8): 17,735-17,745.

Backus, G.E., 1968. Kinematics of geomagnetic secular variation in a perfectly conducting core. Phil. Trans. R. Soc. Lond., A263: 239-266.

Bloxham, J., 1998. Dynamics of angular momentum in the Earth's core. Ann. Rev. Earth Planet. Sci., 26: 501-501.

Braginsky, S.I., 1970. Torsional magnetohydrodynamic vibrations in the Earth's core and variations in day length. Geomag. Aeron., 10: 1-8 (Engl. Trans.).

Bullard, E.C. and H. Gellman, 1954. Homogeneous dynamos and terrestrial magnetism. Phil. Trans. R. Soc. Lond., A247: 213-278.

Chave, A.D. and D.S. Luther, 1990. Low-frequency, motionally induced electromagnetic fields in the ocean. J. Geophys. Res., 95(C5): 7185-7200.

Courtillot V. and J.-L. LeMouël, 1998. Time variations of the Earth's magnetic field: from daily to secular. Ann. Rev. Earth Planet. Sci., 16: 389-476.

Flosadóttir, Á.H., J.C. Larsen, and J.T. Smith, 1997. Motional induction in North Atlantic circulation models. J. Geophys. Res., 102: 10353-10372.

Gubbins, D., 1973. Numerical solutions of the dynamo problem. Phil. Trans. Roy. Soc. Lond., A274: 493-521.

Jackson, A., J. Bloxham and D. Gubbins, 1993. Time-dependent flow at the core surface and conservation of angular momentum in the coupled core-mantle system. In: J.-L. LeMouël, D. Dmylie, and T. Herring (Editors). Dynamics of Earth's Deep Interior and Earth Rotation. Am. Geophys. Union, Geophys. Monogr. Ser., 72: 97-107.

Jault, D., C. Gire and J.-L. LeMouël, 1988. Westward drift, core motions and exchanges of angular momentum between core and mantle. Nature, 333: 353-356.

Koyama, T., H. Shimizu and H. Utada, 2002. Possible effects of lateral heterogeneity in the D″layer on electromagnetic variations of core origin, Phys. Earth Planet. Int., 129: 99-116.

Krause, F. and K.H. Rädler, 1980. Mean-Field Magnetohydrodynamics and Dynamo Theory, Academic Press, 271 pp.

Larsen, J.C., 1992. Transport and heat flux of the Florida current at 27∘N derived from cross-stream voltages and profiling data: Theory and observations. Phil. Trans. R. Soc. Lond., A338: 169-236.

Langel, R.A., 1987. The main field. In: J.Jacobs (Editor). Geomagnetism vol.1: 249-512.

Lanzerotti, L.J., L.V. Medford, C.G. Maclennan, D.J. Thomson, A. Meloni, and G.P. Gregori, 1985. Measurements of the large-scale direct-current Earth potential and possible implications for the geomagnetic dynamo. Science, 229: 47-49.

Levy, E.H. and S.J. Pearce, 1991 Steady state toroidal magnetic field at Earth's core-mantle boundary. J. Geophys. Res., B96: 3935-3942.

Moffatt, H.K., 1978. Magnetic Field Generation in Electrically Conducting Fluids. Cambridge University Press, Cambridge, 343 pp.

Parker, E.N., 1955. Hydromagnetic dynamo models. Astrophys. J., 121: 293-314.

Parkinson, W.D. and V.R.S. Hutton, 1989. The electrical conductivity of the Earth. In: J.Jacobs(Editor). Geomagnetism vol.3: 281-321.

Roberts, P.H., 1972. Kinematic Dynamo Models. Phil. Trans. R. Soc. Lond., A272: 663-703.

Roberts, P.H. and G.A. Glatzmaier, 2000. Geodynamo theory and simulations. Rev. Mod. Phys., 72: 1081-1123.

Roberts, P.H. and F.J. Lowes, 1961. Earth currents of deep internal origin. J. Geophys. Res., 66: 1243-1254.

Roberts, P.H. and S. Scott, 1965. On analysis of the secular variation. J. Geomagn. Geoelectr., 17: 137-151.

Roberts, P.H. and M. Stix, 1972. α-effect dynamos, by the Bullard-Gellman formalism. Astron. and Astrophys., 18: 453-466.

Runcorn, S.K., 1954. The Earth's core. Trans. Am. Geophys. Union, 35: 49-78.

Runcorn, S.K., 1964. Measurements of planetary electric currents. Nature, 202: 10-13.

Sanford, T.B., 1971. Motionally induced electric and magnetic fields in the sea. J. Geophys. Res., 76: 3476-3492.

Shankland, T.J., J. Peyronneau, and J.P. Poirier, 1993. Electrical conductivity of the Earth's lower mantle. Nature, 366: 453-455.

Shimizu, H., T. Koyama and H. Utada, 1998. An observational constraint on the strength of the toroidal magnetic field at the CMB by time variation of submarine cable voltages. Geophys. Res. Lett., 25: 4023-4026.

Stacy, F., 1992. Physics of the Earth (3rd ed.). Brookfield Press, Brisbane, 513 pp.

Stommel, H., 1948. The westward intensification of wind-driven ocean currents. Trans., AGU, 29: 202-206.

Utada, H., T. Koyama, H. Shimizu and A.D. Chave, 2003. A semi-global reference model for electrical conductivity in the mid-mantle beneath the north Pacific region. Geophys. Res. Lett., 30(4): 1194, doi:10.1029/2002GL016092.

Yokoyama Y. and T. Yukutake, 1991. Sixty year variation in a time series of the geomagnetic gauss coefficients between 1910 and 1983. J. Geomag. Geoelectr., 43: 563-584.

Appendix A. Boundary condition of T at the CMB

Let's use the solutions of T_n in the mantle (see equation (2.11)) to find the boundary condition for T_n in the core at the CMB. Let T_n^M is T_n for $r_D \le r \le r_a$, T_n^D for $r_c < r < r_D$, and T_n^C for the core. The T_n^M that satisfies the boundary condition at $r = r_a$ is

$$T_n^M = \Lambda_0 (r_a^{-n} r^{n+1} - r_a^{n+1} r^{-n}), \tag{A.1}$$

where Λ_0 is a constant. Using this, we can calculate

$$\frac{1}{\sigma_M}\frac{dT_n^M}{dr} = \frac{\Lambda_0}{\sigma_M}\left[(n+1)\left(\frac{r}{r_a}\right)^n + n\left(\frac{r_a}{r}\right)^{n+1}\right]. \tag{A.2}$$

This may be written as

$$\begin{bmatrix} T_n^M \\ \dfrac{1}{\sigma_M}\dfrac{dT_M}{dr} \end{bmatrix} = \Lambda_0 \begin{bmatrix} r\left(\dfrac{r}{r_a}\right)^n - r_a\left(\dfrac{r_a}{r}\right)^n \\ \dfrac{1}{\sigma_M}\left\{(n+1)\left(\dfrac{r}{r_a}\right)^n + n\left(\dfrac{r_a}{r}\right)^{n+1}\right\} \end{bmatrix} \equiv \Lambda_0 \mathbf{a}_n(r). \tag{A.3}$$

For $r_c \le r \le r_D$,

$$\begin{bmatrix} T_n^D \\ \dfrac{1}{\sigma_D}\dfrac{dT_n^D}{dr} \end{bmatrix} = \begin{bmatrix} r^{n+1} & -r^{-n} \\ \dfrac{n+1}{\sigma_D} r^n & \dfrac{n}{\sigma_D} r^{-(n+1)} \end{bmatrix} \begin{bmatrix} \Lambda_1 \\ \Lambda_2 \end{bmatrix} \equiv \mathbf{D}(r) \begin{bmatrix} \Lambda_1 \\ \Lambda_2 \end{bmatrix}, \tag{A.4}$$

where Λ_1 and Λ_2 are constants. At $r = r_D$, the boundary conditions require

$$\begin{bmatrix} T_n^M \\ \dfrac{1}{\sigma_M}\dfrac{dT_n^M}{dr} \end{bmatrix} = \begin{bmatrix} T_n^D \\ \dfrac{1}{\sigma_D}\dfrac{dT_n^D}{dr} \end{bmatrix}, \tag{A.5}$$

then

$$\begin{bmatrix} \Lambda_1 \\ \Lambda_2 \end{bmatrix} = \Lambda_0 \mathbf{D}_n^{-1}(r_D)\mathbf{a}_n(r_D) \equiv \Lambda_0 \mathbf{A}_n, \tag{A.6}$$

where

$$\mathbf{A}_n = \mathbf{D}_n^{-1}(r_D)\mathbf{a}_n(r_D). \tag{A.7}$$

At $r = r_c$, the boundary conditions imply

$$\begin{bmatrix} T_n^D \\ \dfrac{1}{\sigma_D}\dfrac{dT_n^D}{dr} \end{bmatrix} = \begin{bmatrix} T_n^C \\ \dfrac{1}{\sigma_C}\dfrac{dT_n^C}{dr} \end{bmatrix}, \tag{A.8}$$

and hence

$$\begin{bmatrix} T_n^C \\ \dfrac{1}{\sigma_C}\dfrac{dT_n^C}{dr} \end{bmatrix} = \Lambda_0 \mathbf{D}(r_c)\mathbf{A}_n. \tag{A.9}$$

By eliminating Λ_0 from the expressions of T_C and dT_C/dr, we have the boundary condition for T_C at the CMB. We can write

$$T_n^C(r_c) = \Lambda_0[r_c^{n+1}, \quad -r_c^{-n}]\mathbf{A}_n, \tag{A.10}$$

$$\frac{1}{\sigma_C}\frac{dT_n^C}{dr} = \frac{\Lambda_0}{\sigma_D}[(n+1)r_c^n, \quad nr_c^{-(n+1)}]\mathbf{A}_n. \tag{A.11}$$

By eliminating Λ_0 from above two equations,

$$\frac{T_n^C(r_c)}{\sigma_D}[(n+1)r_c^n, \quad nr_c^{-(n+1)}]\mathbf{A}_n = \frac{1}{\sigma_c}\frac{dT_n^C}{dr}[r_c^{n+1}, \quad -r_c^{-n}]\mathbf{A}_n, \tag{A.12}$$

Hence

$$\frac{\sigma_D}{\sigma_c}\frac{dT_n^C}{dr}[r_c^{n+1}, \quad -r_c^{-n}]\mathbf{A}_n - T_n^C(r_c)[(n+1)r_c^n, \quad nr_c^{-(n+1)}]\mathbf{A}_n = 0. \tag{A.13}$$

This relationship may be written as

$$T_n^C + \Lambda_n\frac{\partial T_n^C}{\partial r} = 0, \tag{A.14}$$

where

$$\Lambda_n = -\frac{\sigma_D}{\sigma_C}\frac{[r_c^{n+1}, -r_c^{-n}]\mathbf{A}_n}{[(n+1)r_c^n, nr_c^{-(n+1)}]\mathbf{A}_n} \tag{A.15}$$

and

$$\mathbf{A}_n = \frac{1}{2n+1}\begin{pmatrix} \frac{n}{r_a^n}\left(1-\left(\frac{r_a}{r_D}\right)^{2n+1}\right) + \frac{\sigma_D}{\sigma_M}\frac{1}{r_a^n}\left((n+1)+n\left(\frac{r_a}{r_D}\right)^{2n+1}\right) \\ (n+1)r_a^{n+1}\left(1-\left(\frac{r_D}{r_a}\right)^{2n+1}\right) + \frac{\sigma_D}{\sigma_M}r_a^{n+1}\left(n+(n+1)\left(\frac{r_D}{r_a}\right)^{2n+1}\right) \end{pmatrix}. \tag{A.16}$$

Appendix B. Demonstration of the convergence of the numerical solutions of the oscillatory dynamo

Convergence of the numerical solutions for the steady kinematic dynamos may be shown by using eigenvalues and eigenfunctions (eigenvectors) arising in the eigenvalue problem. However, eigenvalues cannot be used for the purpose for the oscillatory dynamo problem considered in this paper. We are going to demonstrate the convergence of the solutions by showing the amplitude ratios of the magnetic field variations and Φ (see eq.(3.6)) of oscillatory dynamos obtained by using two different sets of grid.

The two sets of grid employed for the convergence test are (1)$\Delta r = 1/100$ and truncation degree 8 (which is used throughout in the main body of the paper, and will name the grid as G8.100) and (2) $\Delta r = 1/200$ and truncation degree 12 (grid G12.200). The electrical conductivity and the thickness of the D$''$-layer are set as 100S/m and 200km, respectively. Both flows (flow 1 and 2 in Figure 3) are tested, and the magnetic Reynolds numbers used in the test are 1,000 and 3,000.

Table B1 shows the amplitudes of the dipole field oscillation ($\Delta S_1/S_1$), and Table B2 lists the amplitude ratios $\Delta T_2/\Delta S_1$ at the CMB for all the combinations of grids, flows and R_m's. The differences of the values of the ratios due to different grids are at most a few per cent for each combination of the flow and R_m. Figures B1 and B2 show the Φ's with $R_m = 1,000$ and 3,000, respectively. Slight difference may be seen in the Φ with flow 1, but corresponding distributions have common features representing characteristics of Φ generated by the flows. Therefore, we concluded that the numerical results shown in main body of the paper are convergent (at least within the accuracy of the discussions in this paper).

Tables

Table 1. The ratio of the principle toroidal to poloidal magnetic field at the CMB.

d (km)	σ_D (S/m)	Conductance (S)	T_2/S_1 at the CMB
200	5×10	1×10^7	1.44×10^{-4}
200	1×10^2	2×10^7	2.69×10^{-4}
200	1×10^3	2×10^8	2.51×10^{-3}
200	1×10^4	2×10^9	2.48×10^{-2}
200	1×10^5	2×10^{10}	2.32×10^{-1}
100	1×10^2	1×10^7	1.45×10^{-4}
500	1×10^2	5×10^7	6.23×10^{-4}

Table 2. Ratio of the amplitude of oscillation of toroidal to poloidal magnetic field at the CMB ($\Delta T_2/\Delta S_1$). Oscillation period and R_m are set to 30 years and 1,000, respectively.

d (km)	σ_D (S/m)	Conductance (S)	flow1	flow2
200	5×10	1×10^7	0.72	0.58
200	1×10^2	2×10^7	1.36	1.09
200	1×10^3	2×10^8	12.62	10.08
200	1×10^4	2×10^9	118.31	94.62
100	1×10^2	1×10^7	0.73	0.58
500	1×10^2	5×10^7	3.14	2.51

Table 3. Induced electric field by external field variations

period	ΔB (nT)	Length scale (km)	ΔE^F (mV/km)	V^F	ΔE^{MT} (mV/km)	V^{MT}
1 day	50	5000	1.8×10^1	18V	4.8×10^{-1}	0.48V
6 months	10	10000	4.0×10^{-2}	40mV	7.1×10^{-3}	7.1mV
1 year	10	10000	2.0×10^{-2}	20mV	5.0×10^{-3}	5.0mV
11 years	10	10000	1.8×10^{-3}	1.8mV	1.5×10^{-3}	1.5mV

Table B1. Relative amplitude of the dipole field oscillation ($\Delta S_1/S_1$).

	flow1		flow2	
	$R_m = 1,000$	$R_m = 3,000$	$R_m = 1,000$	$R_m = 3,000$
G8.100	4.63×10^{-4}	1.43×10^{-3}	5.74×10^{-4}	1.58×10^{-3}
G12.200	4.53×10^{-4}	1.31×10^{-3}	5.77×10^{-4}	1.62×10^{-3}

Table B2. The amplitude ratio of the principle toroidal to poloidal magnetic field variations at the CMB obtained using two sets of grids.

	flow1		flow2	
	$R_m = 1,000$	$R_m = 3,000$	$R_m = 1,000$	$R_m = 3,000$
G8.100	1.36	1.38	1.09	1.17
G12.200	1.32	1.33	1.10	1.19

Figure Captions

Figure 1. Network of the submarine cables for geoelectric observations in the western Pacific.

Figure 2. The kinematic dynamo model. The mantle is two-layered and electrically conducting.

Figure 3. Angular velocity distributions, relative to the CMB, of the applied zonal oscillatory flows (eq.(2.25) and (2.26)). Flow 1 has stronger shear beneath the polar region and Flow 2 has one blew the equator.

Figure 4. Thickness and electrical conductivity of the D″layer, d and σ_D, respectively, used in the calculations.

Figure 5. Eigenfunctions of T_2 and S_1 of the steady α^2 dynamo with $\sigma_D = 10^2$, 10^4, and 10^5 S/m. $d = 200$ km in all cases. Almost no differences may be seen in S_1's. T_2's are not 0 at the CMB ($r = 1$), but the value is significant only if the electrical conductivity of the D″-layer is very high (as high as 10^5 S/m, which is not plausible for the D″-layer).

Figure 6. The relationship between the ratio of the lowest mode of the toroidal and poloidal magnetic field at the CMB generated by the steady α^2 dynamo and the conductance of the D″layer. The ratio is determined by the conductance, not by the conductivity, of the D″-layer.

Figure 7. Time series of the first few modes of the magnetic field at the CMB generated by the perturbed dynamo. The zonal oscillatory flow used for the calculation is flow 2 (see Fig.3). $R_\alpha = R_{\alpha cr}$, $d = 200$km, $\sigma_D = 100$ S/m, $R_m = 1000$.

Figure 8. The relationship between R_m and the amplitude of the dipole oscillation, $\Delta S_1/S_1$, generated by the two flows.

Figure 9. The relationship between the ratio $\Delta T_2/\Delta S_1$ and the conductance of the D″layer. The ratio is determined by the conductance, not by the conductivity, of the D″-layer.

Figure 10. Expected voltage variation produced by flow 2 and measured by existing cable network and a fictitious cable between 55-35 degree latitude. $R_\alpha = R_{\alpha cr}$, $d = 200$km, $\sigma_D = 100$ S/m, $R_m = 1000$.

Figure 11. Φ by the two oscillating flows. The locations of high gradients in Φ are very different due to the difference of the locations of strong shear in flow 1 and 2. $R_\alpha = R_{\alpha cr}$, $d = 200$km, $\sigma_D = 100$ S/m, $R_m = 1000$.

Figure 12. Change of Φ distribution due to different conductivity in the D″layer. Flow 2 and $R_m = 1000$ are used for the calculation.

Figure 13. Change of Φ distribution due to R_m. Flow 2, $d = 200$ km, $\sigma_D = 100$ S/m are used for the calculation.

Figure 14. Streamline of the ocean circulation in a flat rectangular model ocean based on Stommel(1948). Contour interval is 10sv (1sv=10^6m^3/s).

Figure 15. Distribution of the electric potential induced by the model ocean current in Fig.14 and axial dipole geomagnetic field (g_1^0=-30,000nT). Electric potential is set zero at 3150km on the western (left) boundary. Contour interval is 0.05V.

Figure B1. Comparison of Φ calculated using different sets of grid (G8.100 and G12.200) with $R_m = 1,000$. ($R_\alpha = R_{\alpha cr}$, $d = 200$km, $\sigma_D = 100$ S/m.)

Figure B2. Comparison of Φ calculated using different sets of grid (G8.100 and G12.200) with $R_m = 3,000$. ($R_\alpha = R_{\alpha cr}$, $d = 200$km, $\sigma_D = 100$ S/m.)

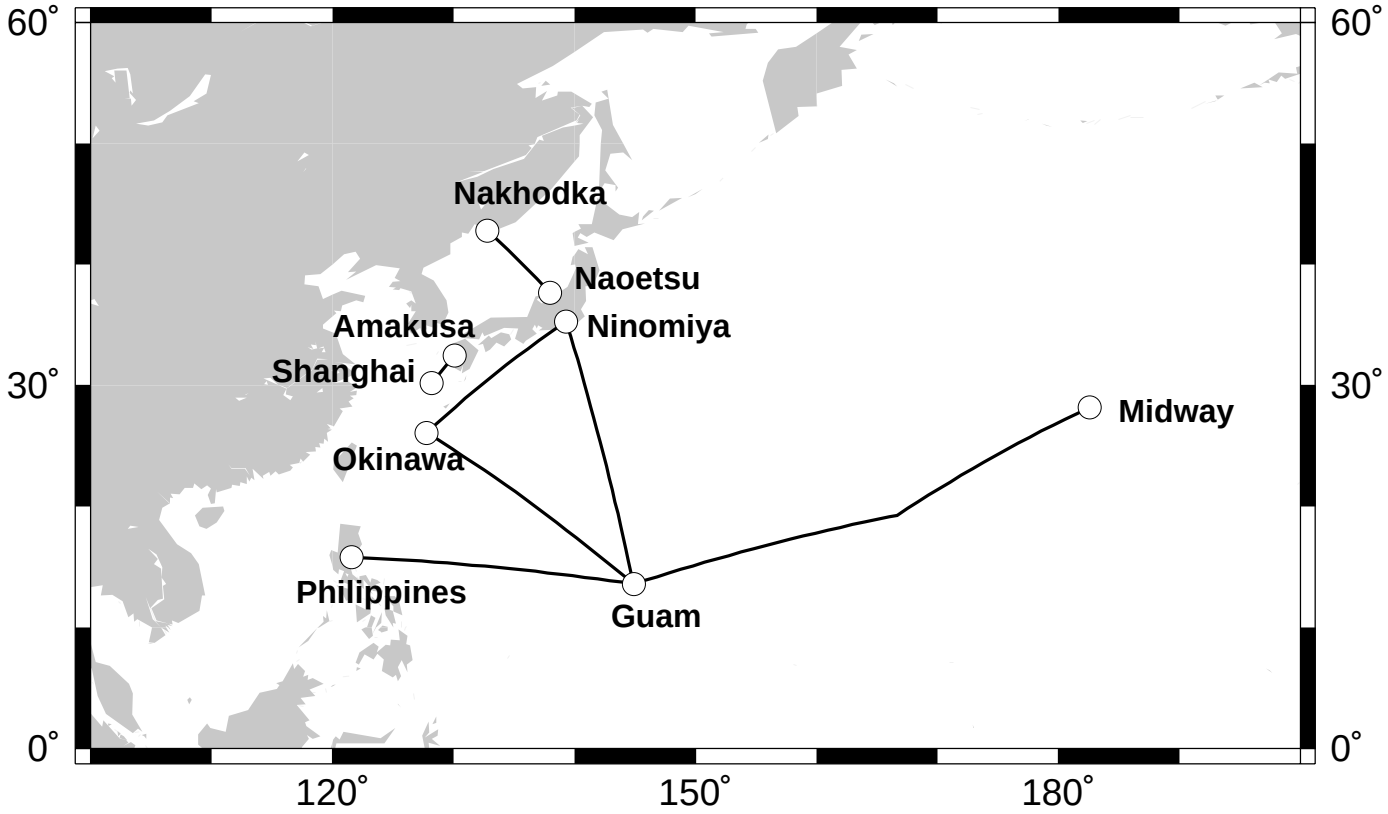
60˚
60˚
30˚
30˚
0˚
0˚
120˚
150˚
180˚
Nakhodka
Naoetsu
Amakusa
Ninomiya
Shanghai
Midway
Okinawa
Philippines
Guam

Figure 1

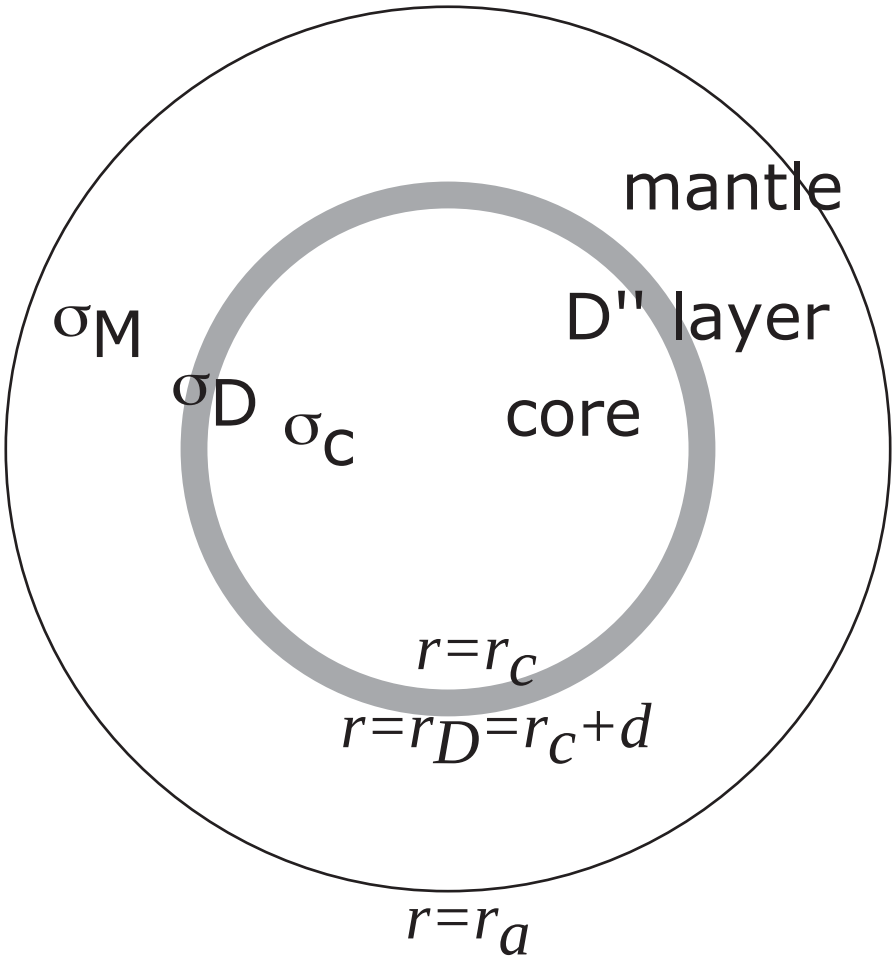

Figure 2

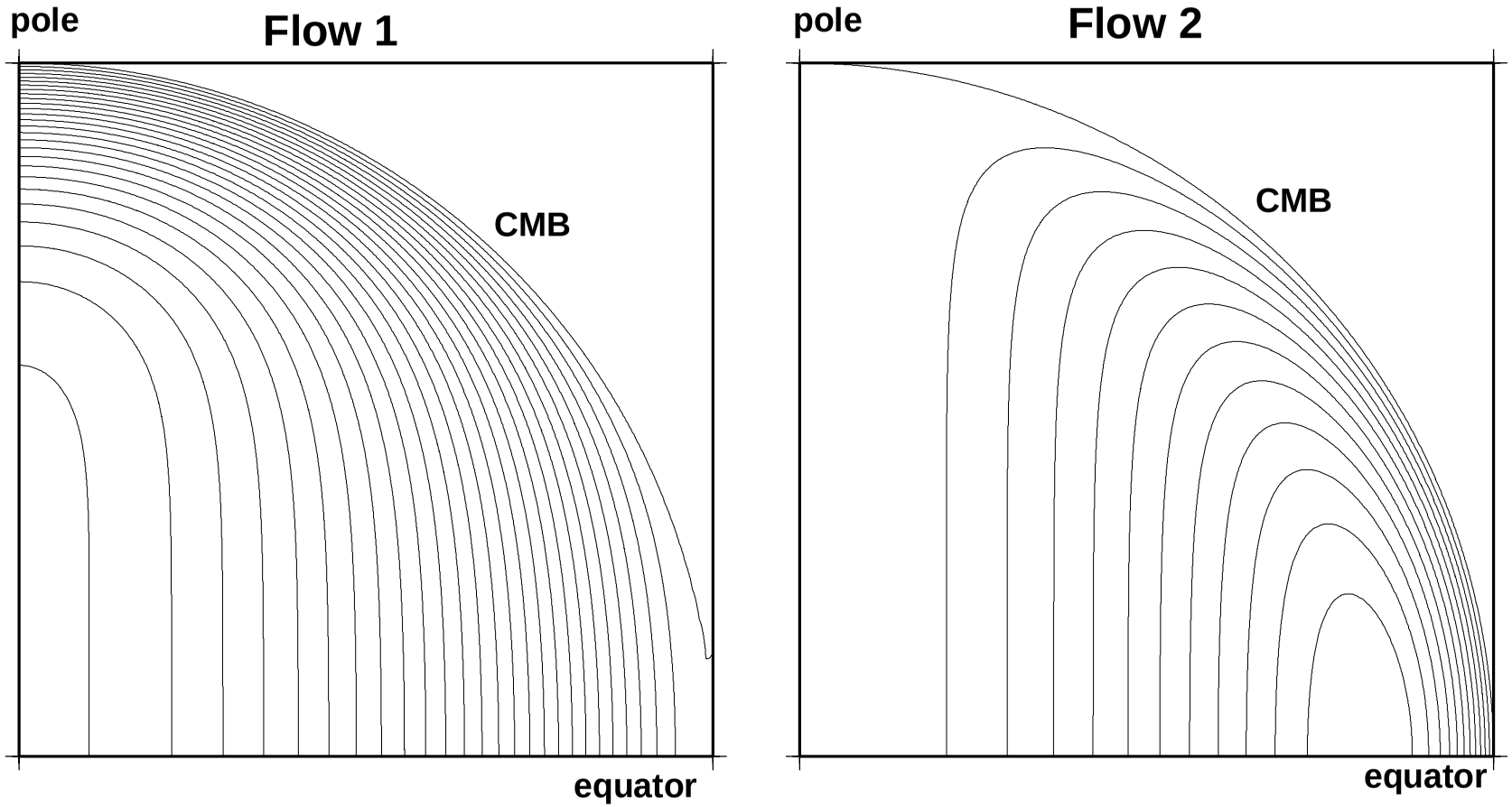

Figure 3

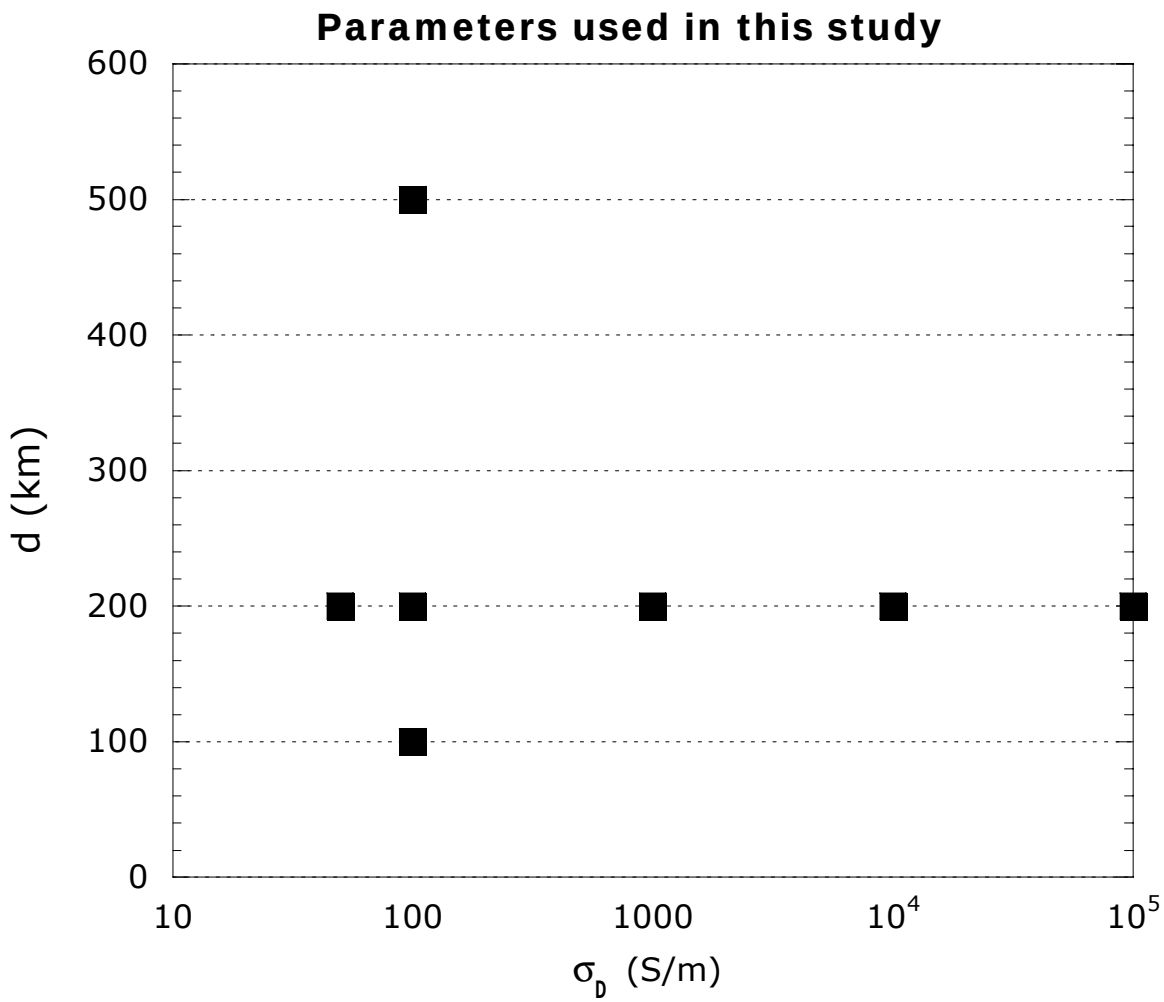
Parameters used in this study
600
500
400
300
200
100
0
d (km)
10
100
1000
10^4
10^5
σ_D (S/m)

Figure 4

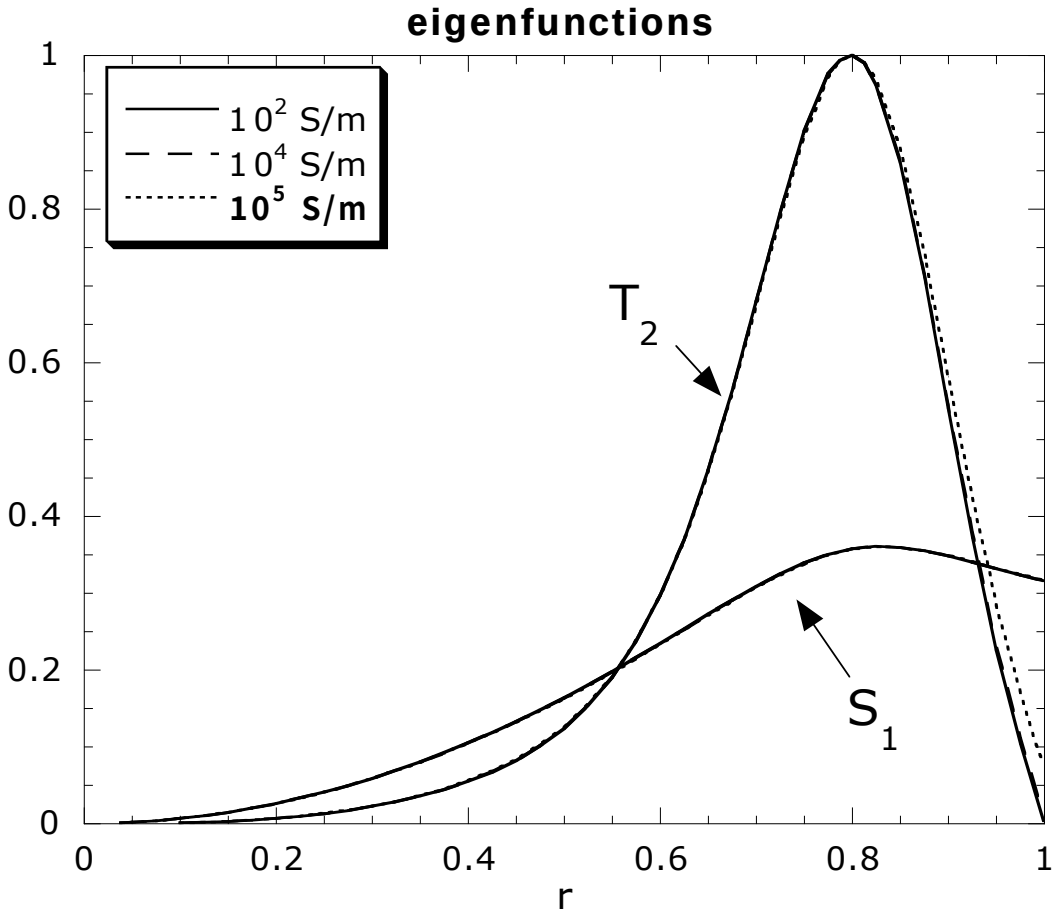
eigenfunctions
10^2 S/m
10^4 S/m
10^5 S/m
T2
S1
1
0.8
0.6
0.4
0.2
0
0
0.2
0.4
0.6
0.8
1
r

Figure 5

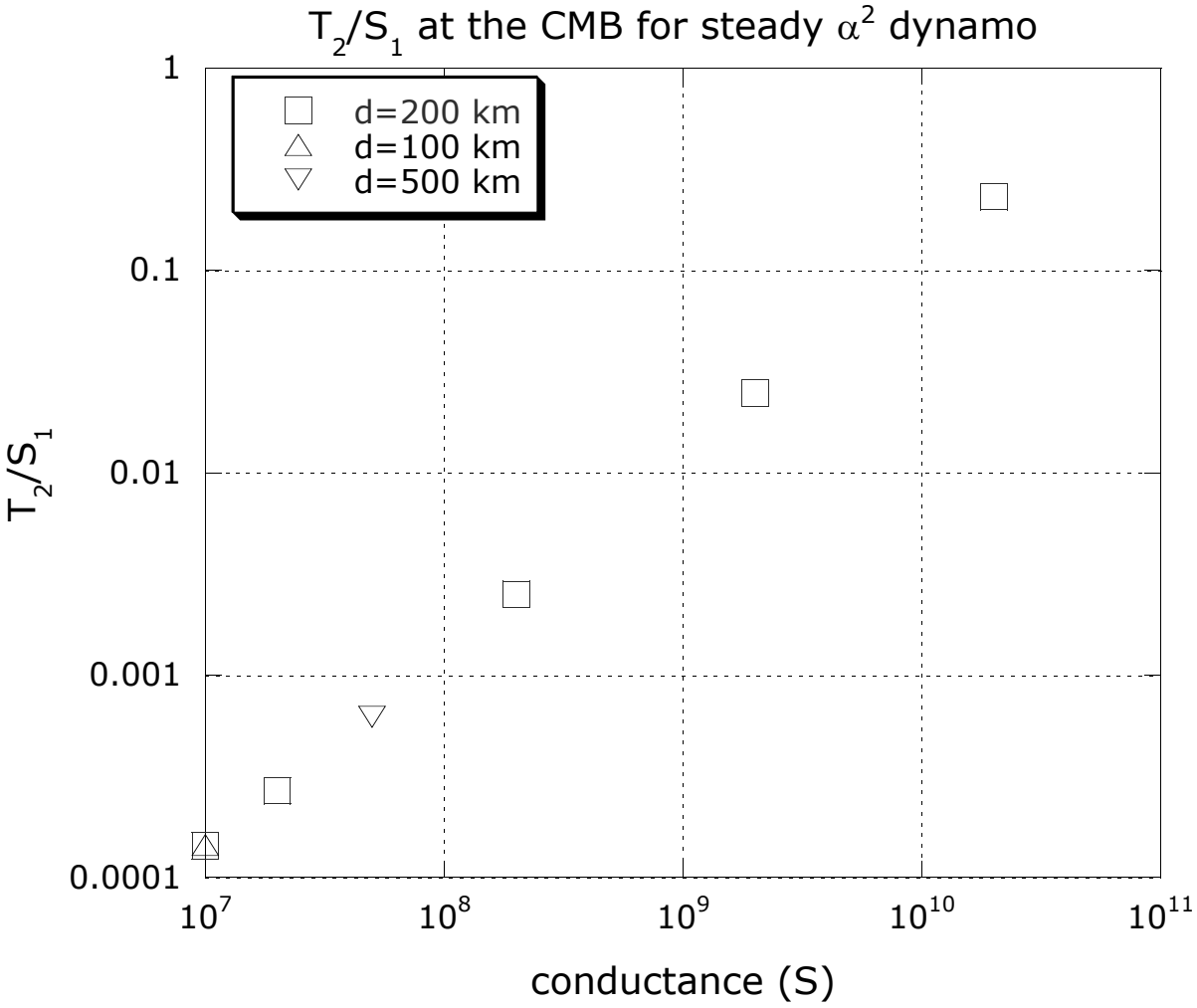
T2/S1 at the CMB for steady α2 dynamo
d=200 km
d=100 km
d=500 km
1
0.1
0.01
0.001
0.0001
T2/S1
10^7
10^8
10^9
10^10
10^11
conductance (S)

Figure 6

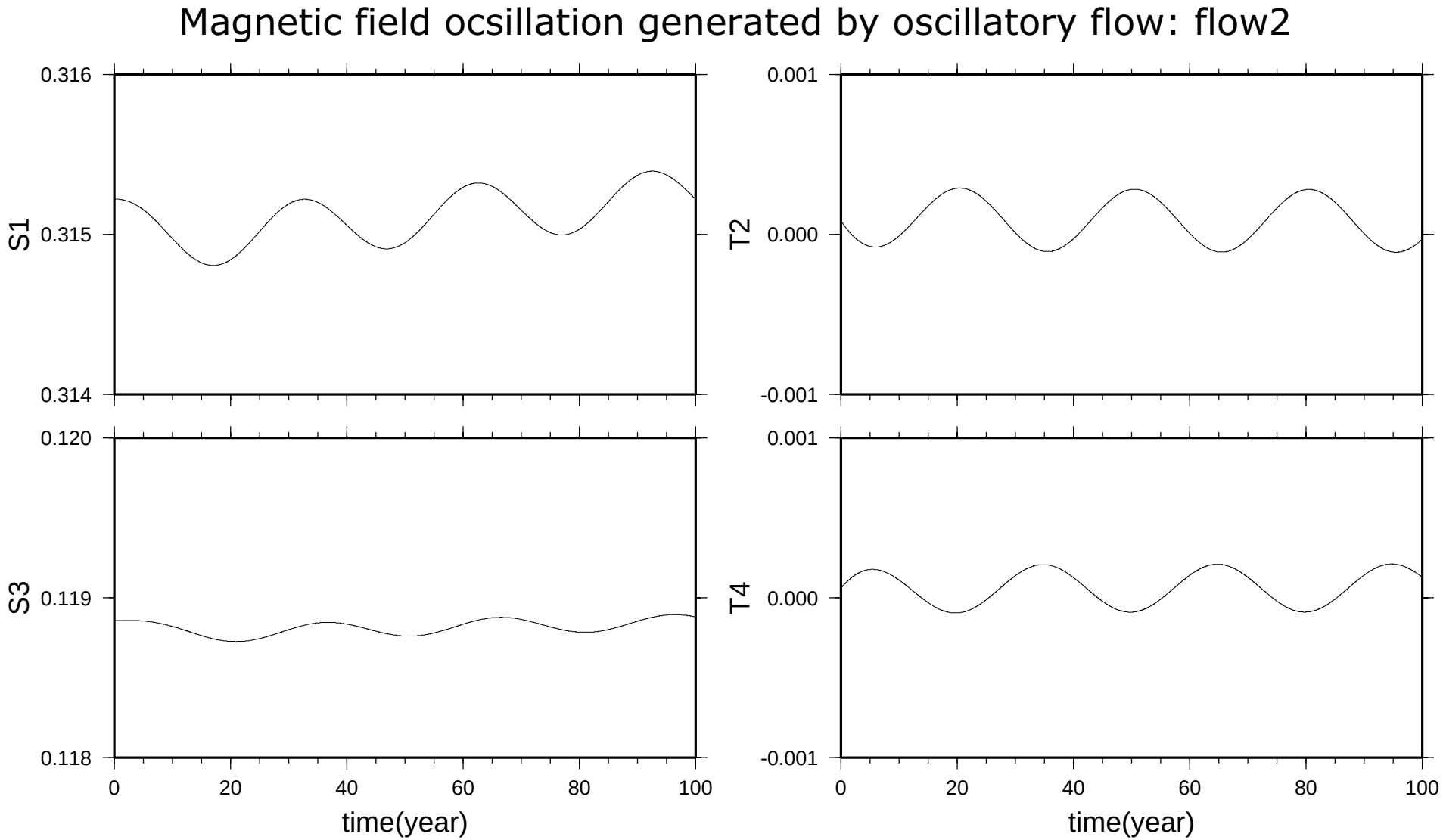
Magnetic field ocsillation generated by oscillatory flow: flow2
S1
0.316
0.315
0.314
T2
0.001
0.000
-0.001
S3
0.120
0.119
0.118
T4
0.001
0.000
-0.001
0
20
40
60
80
100
time(year)
time(year)

Figure 7

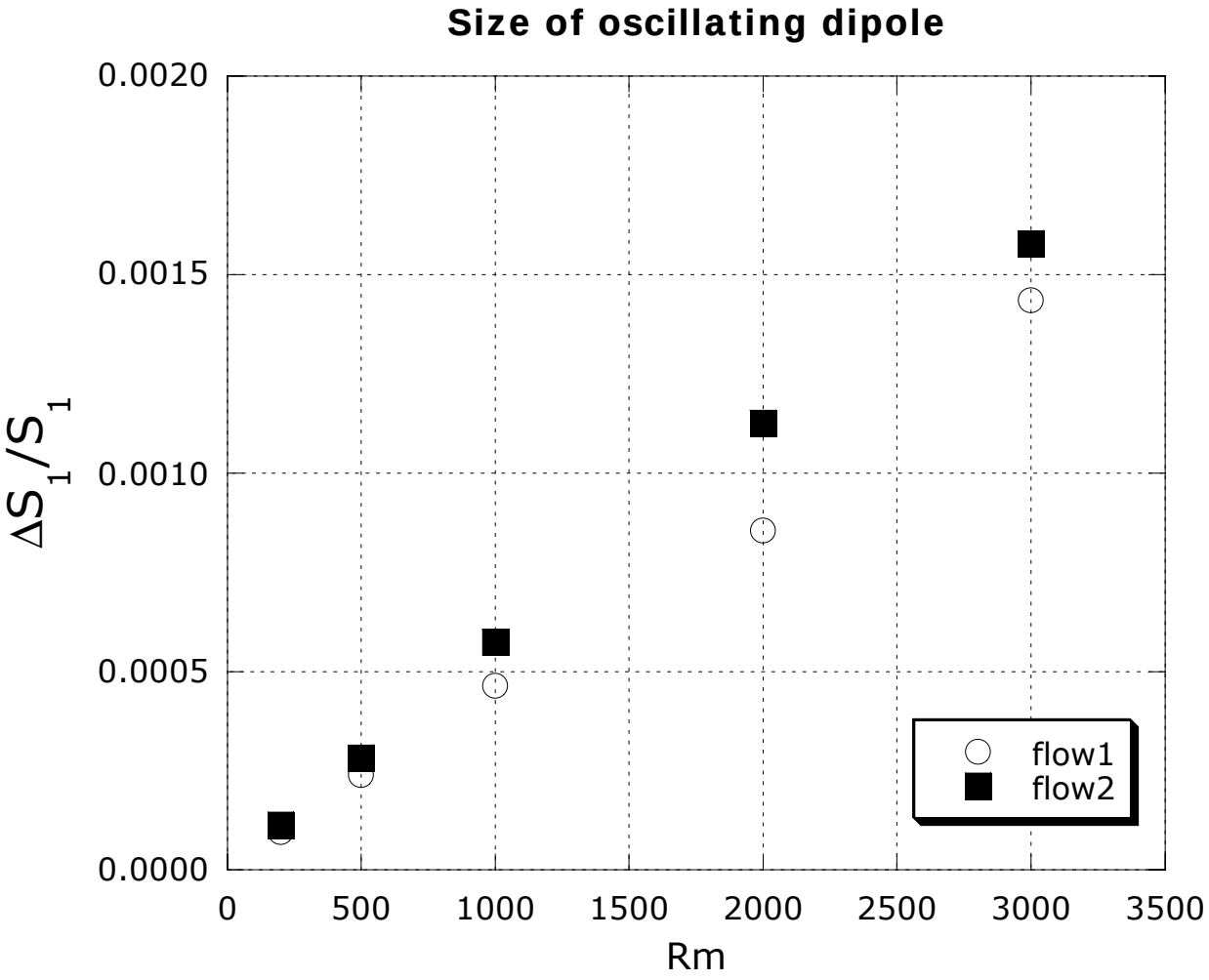
Size of oscillating dipole
0.0020
0.0015
0.0010
0.0005
0.0000
$\Delta S_1/S_1$
0
500
1000
1500
2000
2500
3000
3500
Rm
flow1
flow2

Figure 8

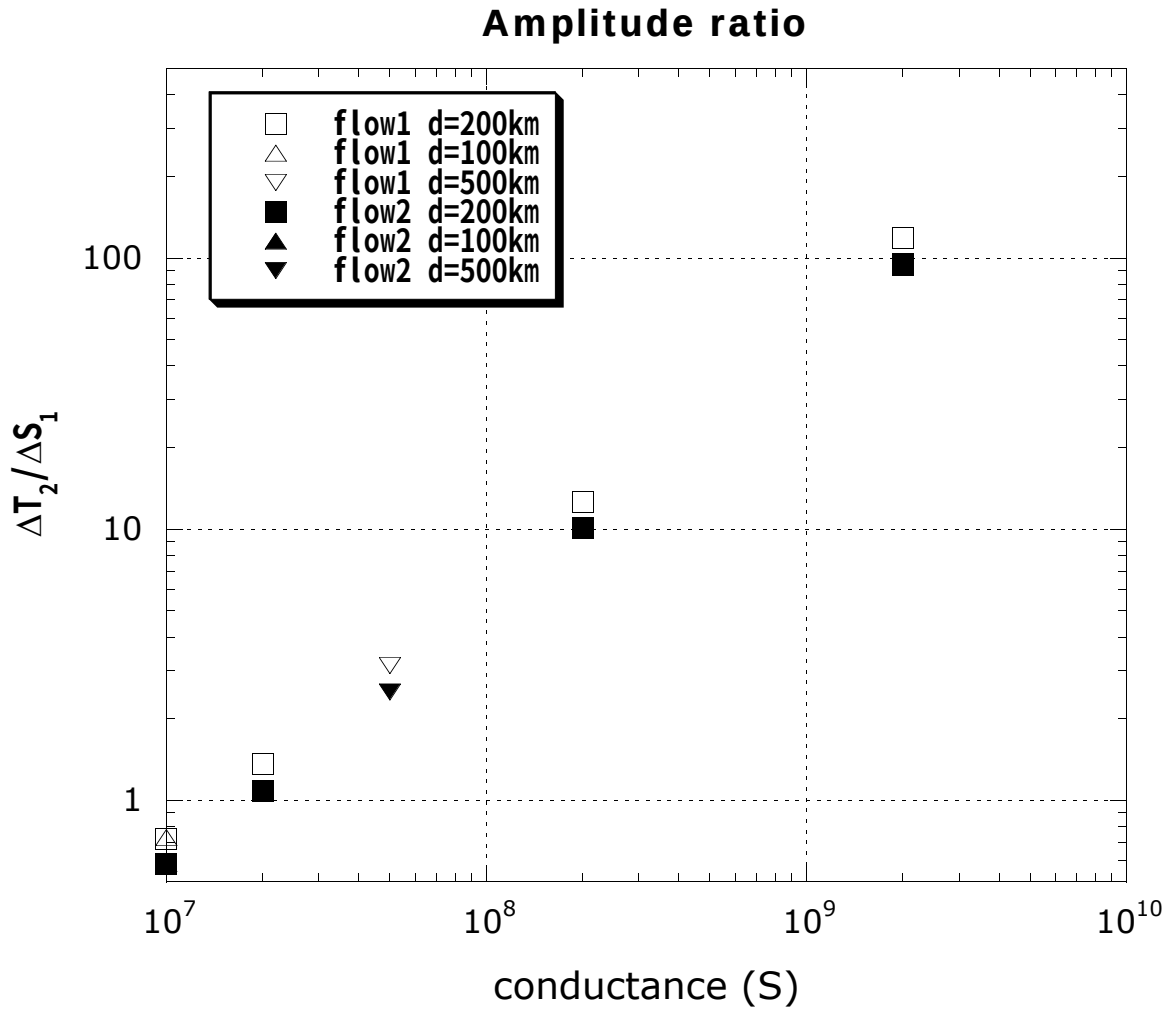
Amplitude ratio
flow1 d=200km
flow1 d=100km
flow1 d=500km
flow2 d=200km
flow2 d=100km
flow2 d=500km
100
10
1
$\Delta T_2/\Delta S_1$
10^7
10^8
10^9
10^{10}
conductance (S)

Figure 9

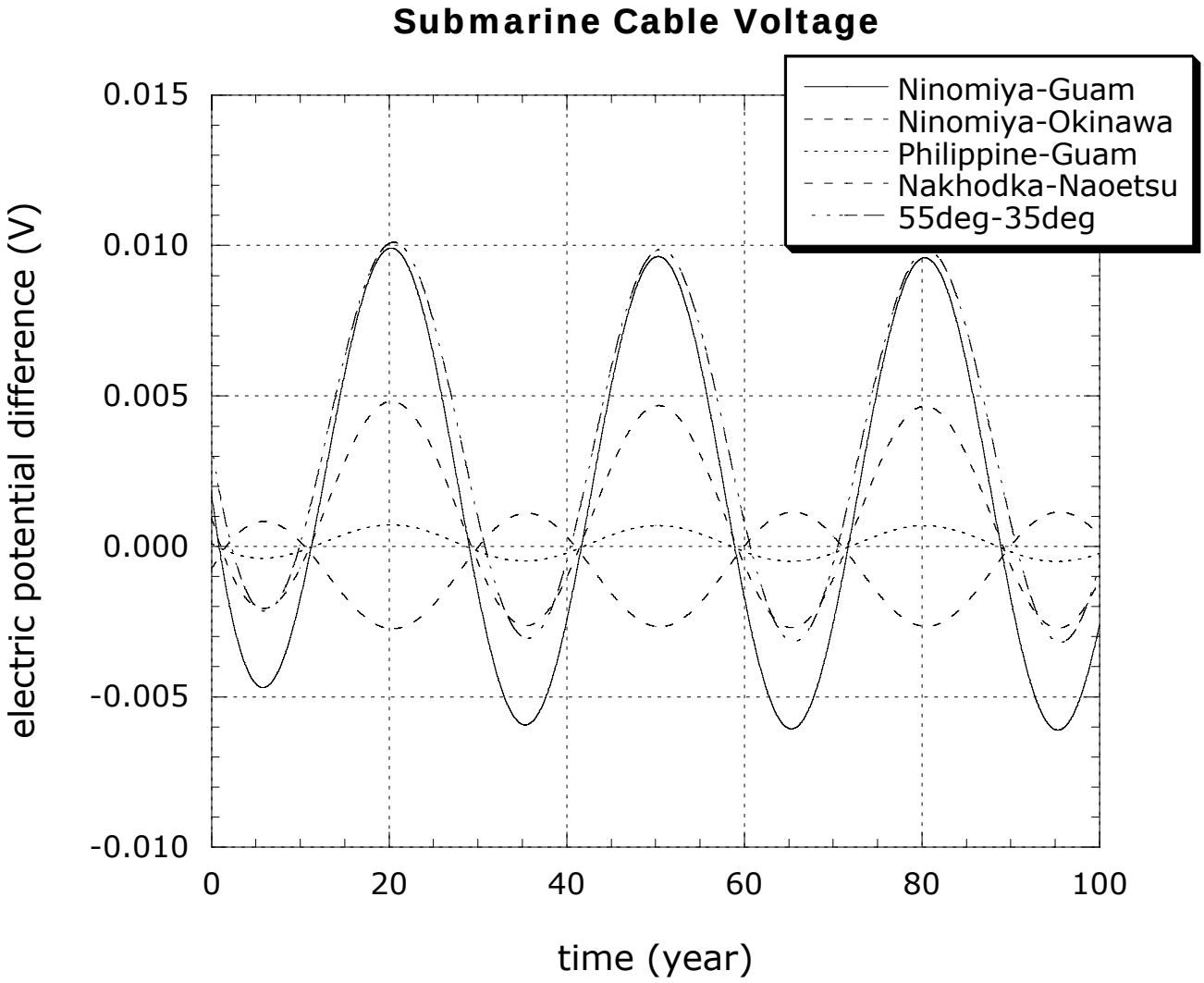
Submarine Cable Voltage
Ninomiya-Guam
Ninomiya-Okinawa
Philippine-Guam
Nakhodka-Naoetsu
55deg-35deg
0.015
0.010
0.005
0.000
-0.005
-0.010
electric potential difference (V)
0
20
40
60
80
100
time (year)

Figure 10

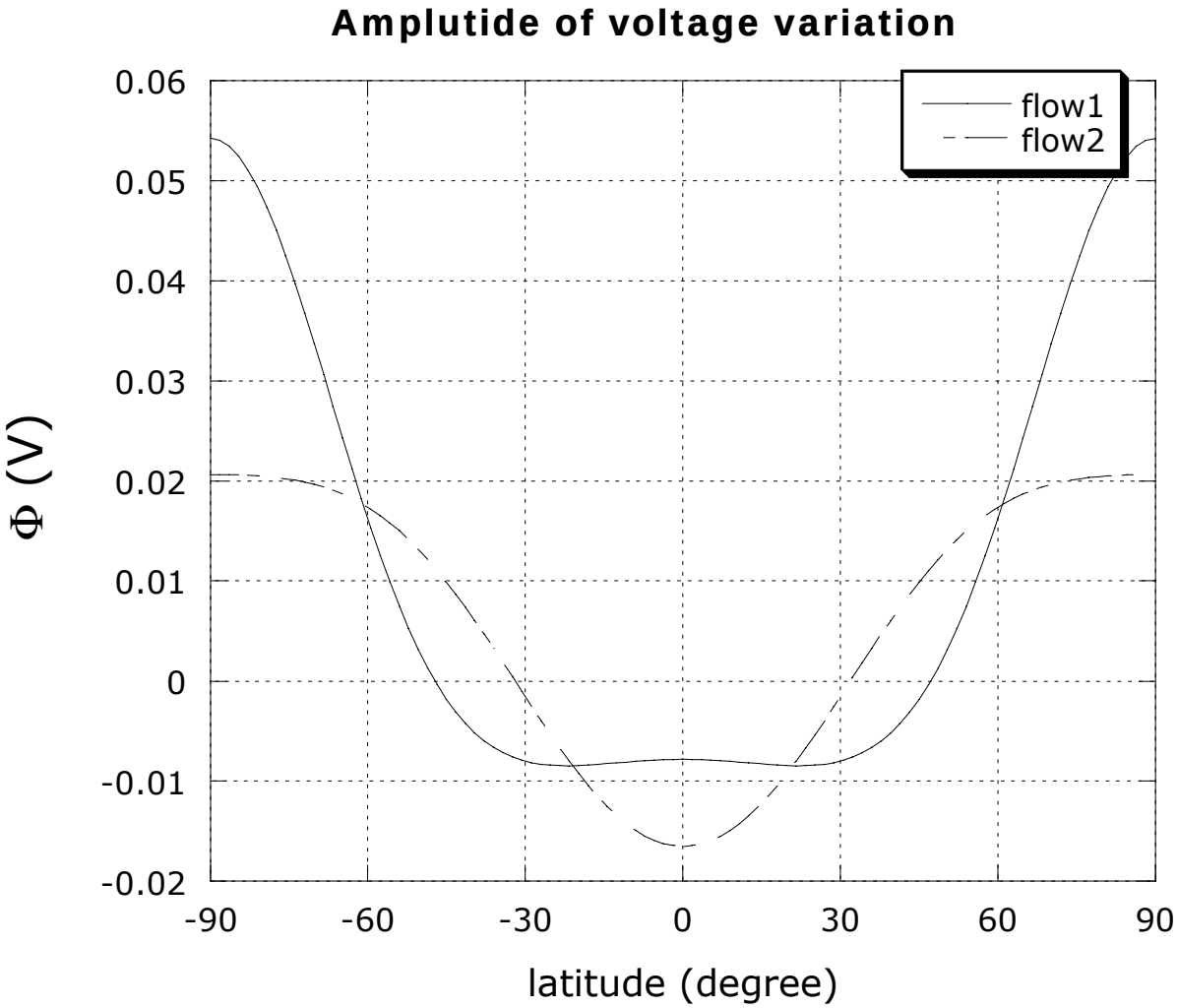
Amplutide of voltage variation
flow1
flow2
0.06
0.05
0.04
0.03
0.02
0.01
0
-0.01
-0.02
Φ (V)
-90
-60
-30
0
30
60
90
latitude (degree)

Figure 11

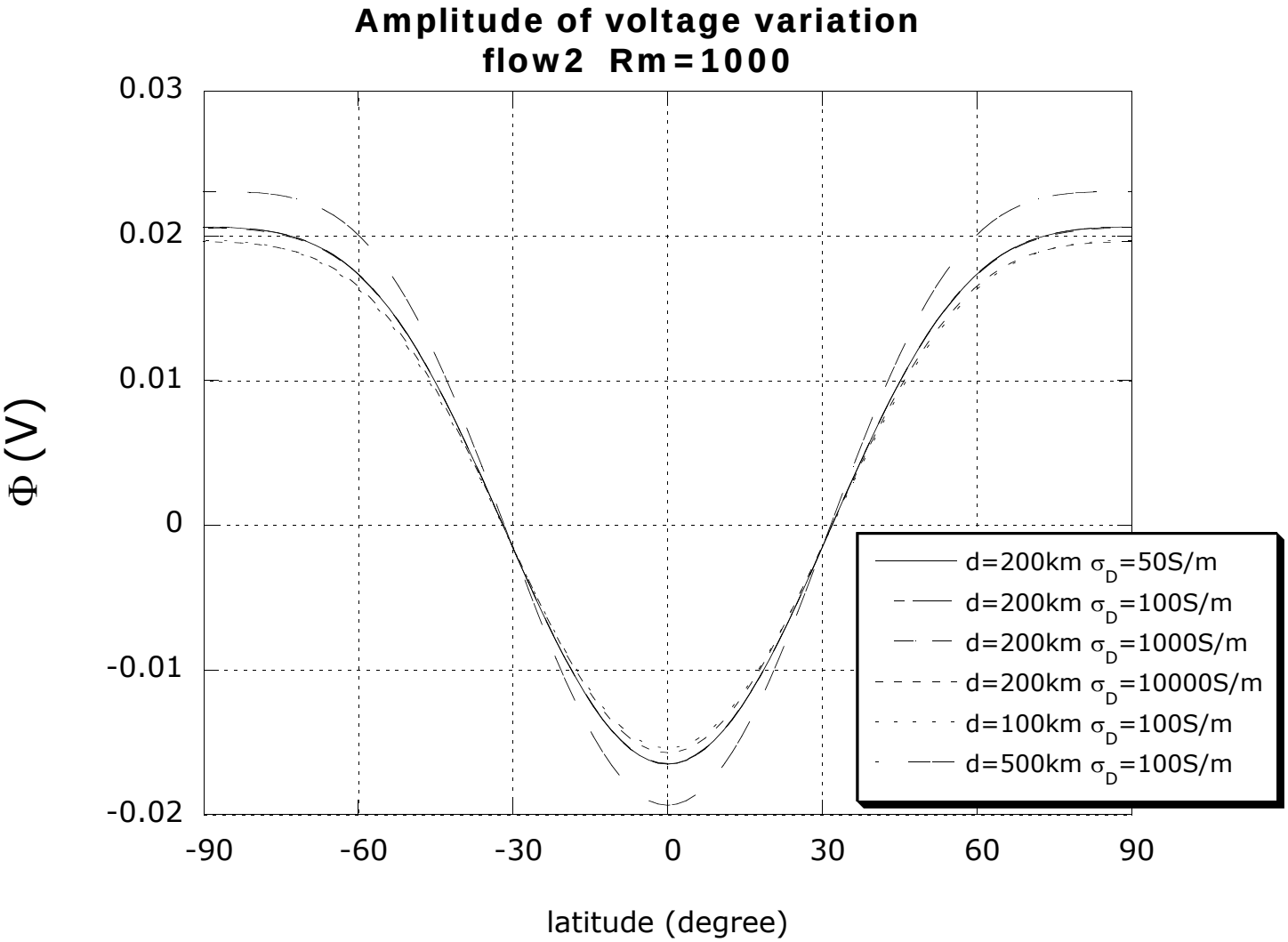
Amplitude of voltage variation
flow2 Rm=1000
0.03
0.02
0.01
0
-0.01
-0.02
Φ (V)
-90
-60
-30
0
30
60
90
latitude (degree)
d=200km σD=50S/m
d=200km σD=100S/m
d=200km σD=1000S/m
d=200km σD=10000S/m
d=100km σD=100S/m
d=500km σD=100S/m

Figure 12

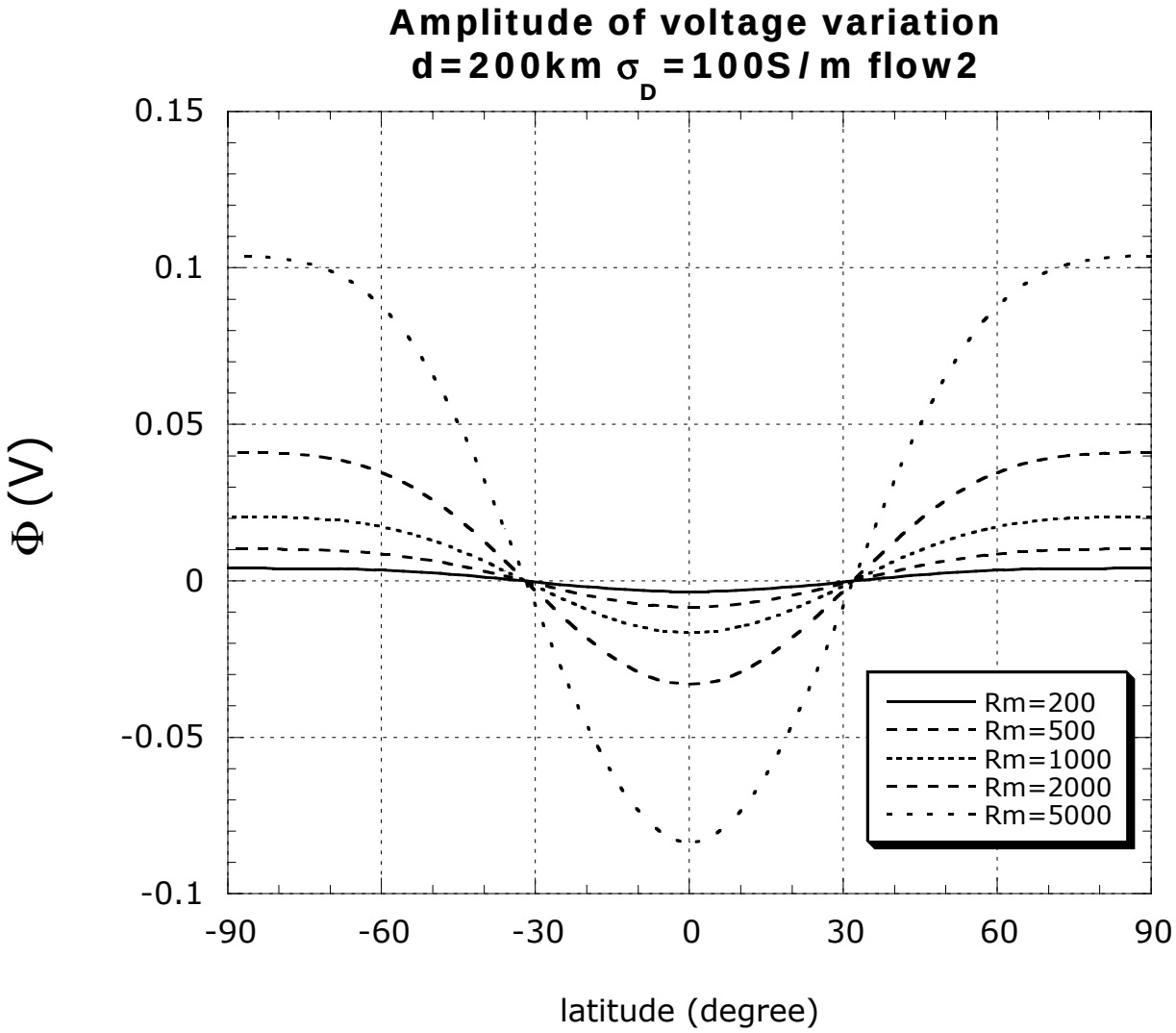
Amplitude of voltage variation
d=200km σD=100S/m flow2
Φ (V)
0.15
0.1
0.05
0
-0.05
-0.1
-90
-60
-30
0
30
60
90
latitude (degree)
Rm=200
Rm=500
Rm=1000
Rm=2000
Rm=5000

Figure 13

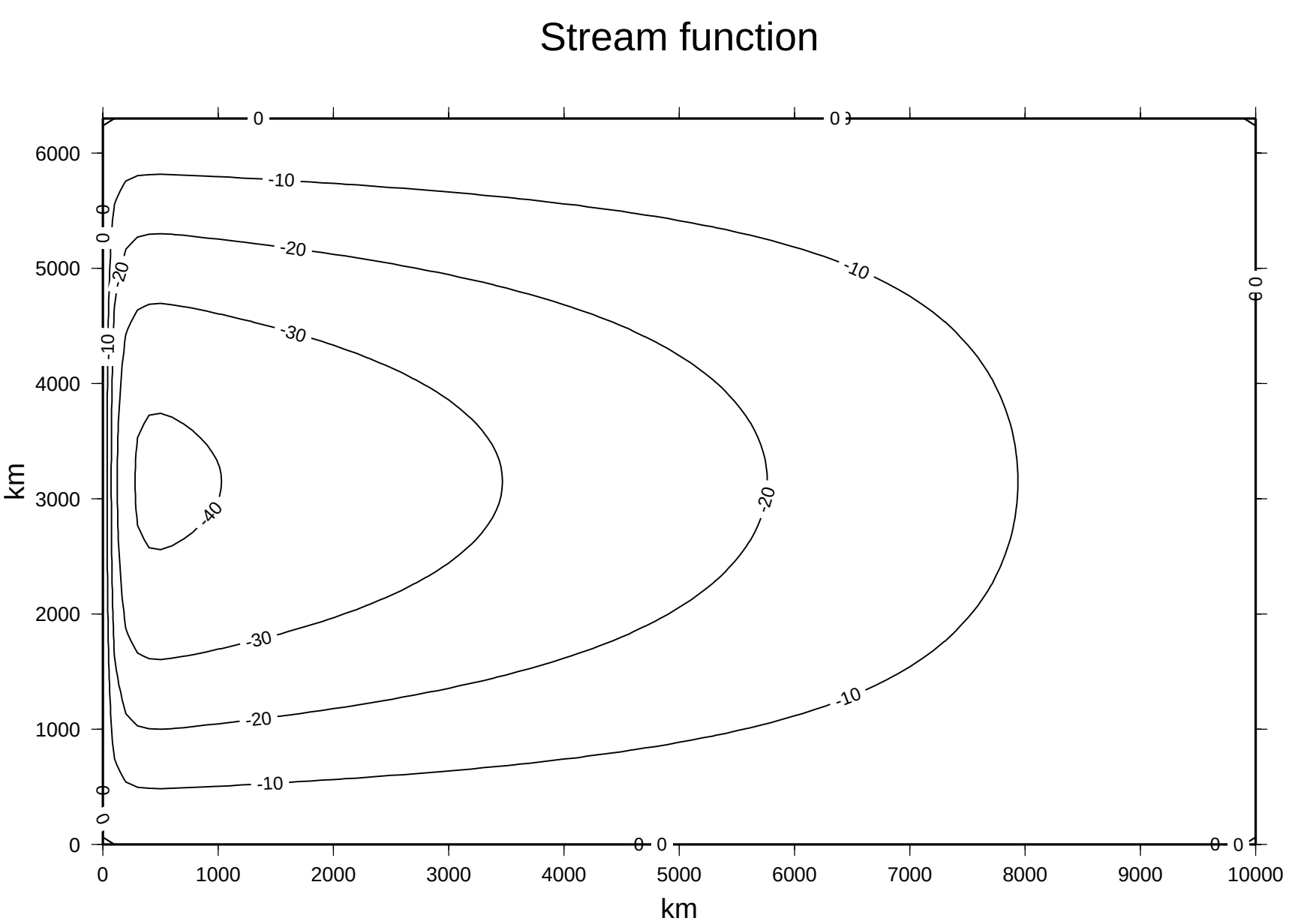
Stream function
km
km
0
1000
2000
3000
4000
5000
6000
7000
8000
9000
10000
-10
-20
-30
-40

Figure 14□

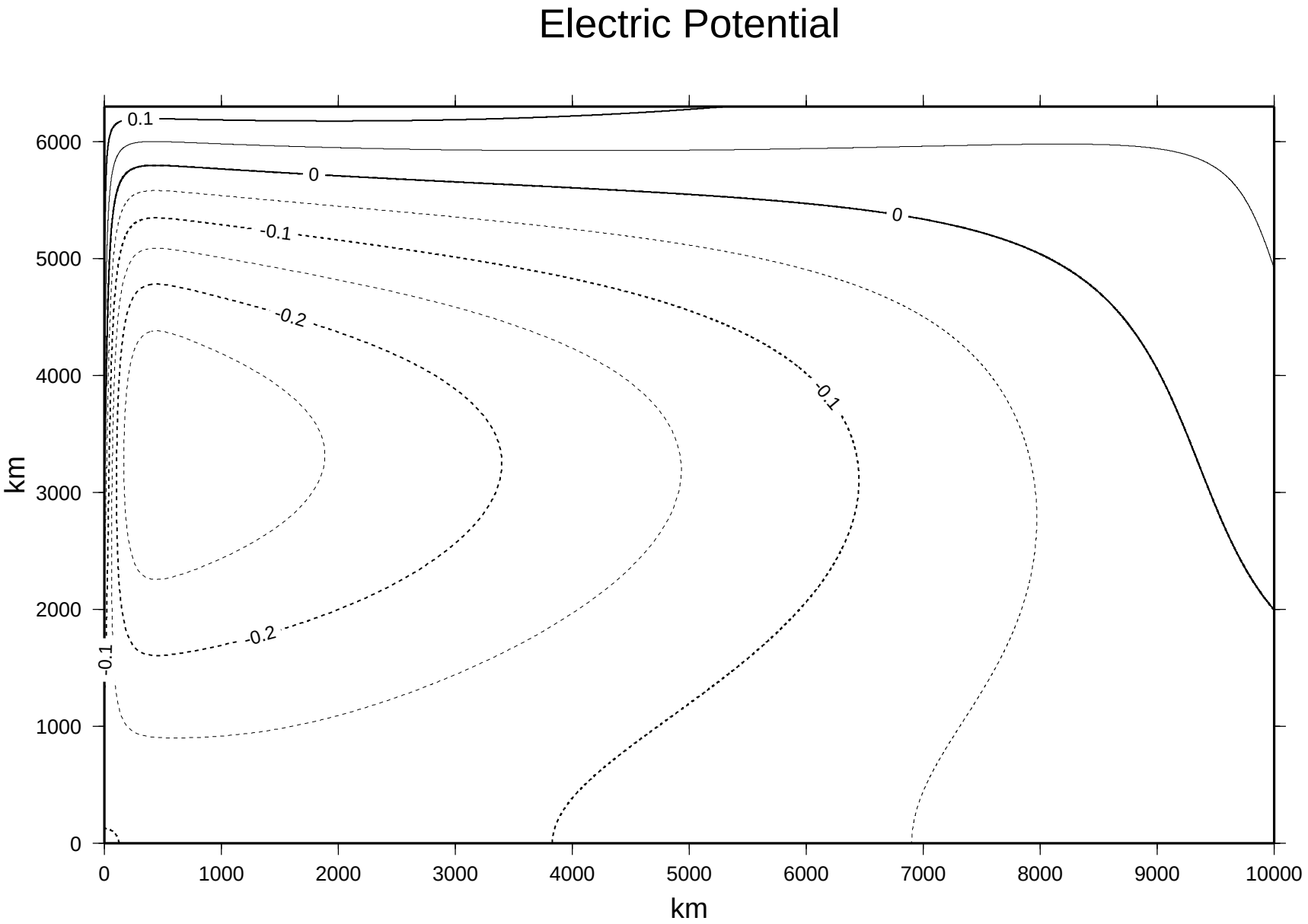
Electric Potential
0.1
0
0
-0.1
-0.2
-0.1
-0.2
-0.1
6000
5000
4000
3000
2000
1000
0
km
0
1000
2000
3000
4000
5000
6000
7000
8000
9000
10000
km

Figure 15

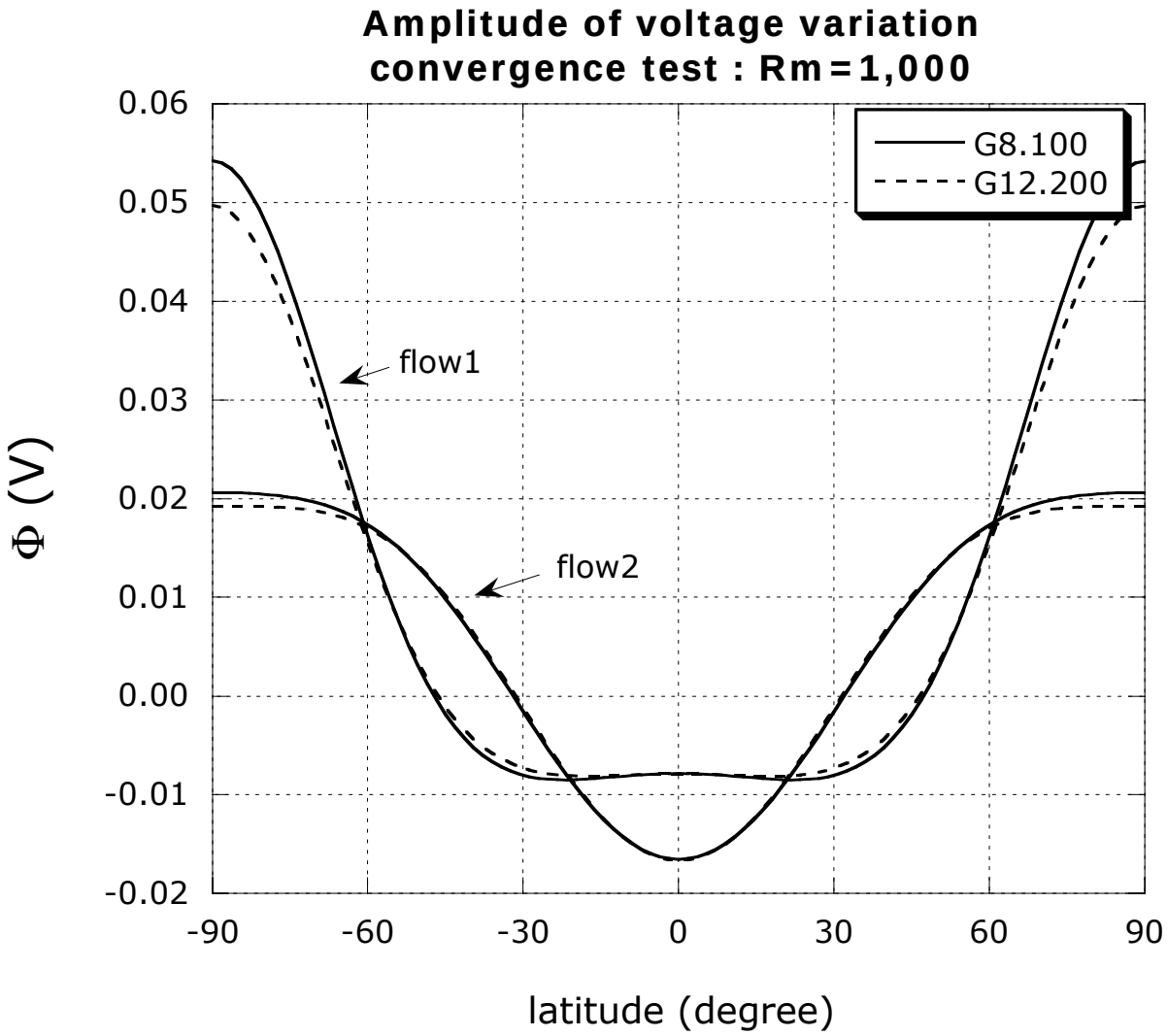
Amplitude of voltage variation
convergence test : Rm=1,000
G8.100
G12.200
flow1
flow2
Φ (V)
0.06
0.05
0.04
0.03
0.02
0.01
0.00
-0.01
-0.02
-90
-60
-30
0
30
60
90
latitude (degree)

Figure B1

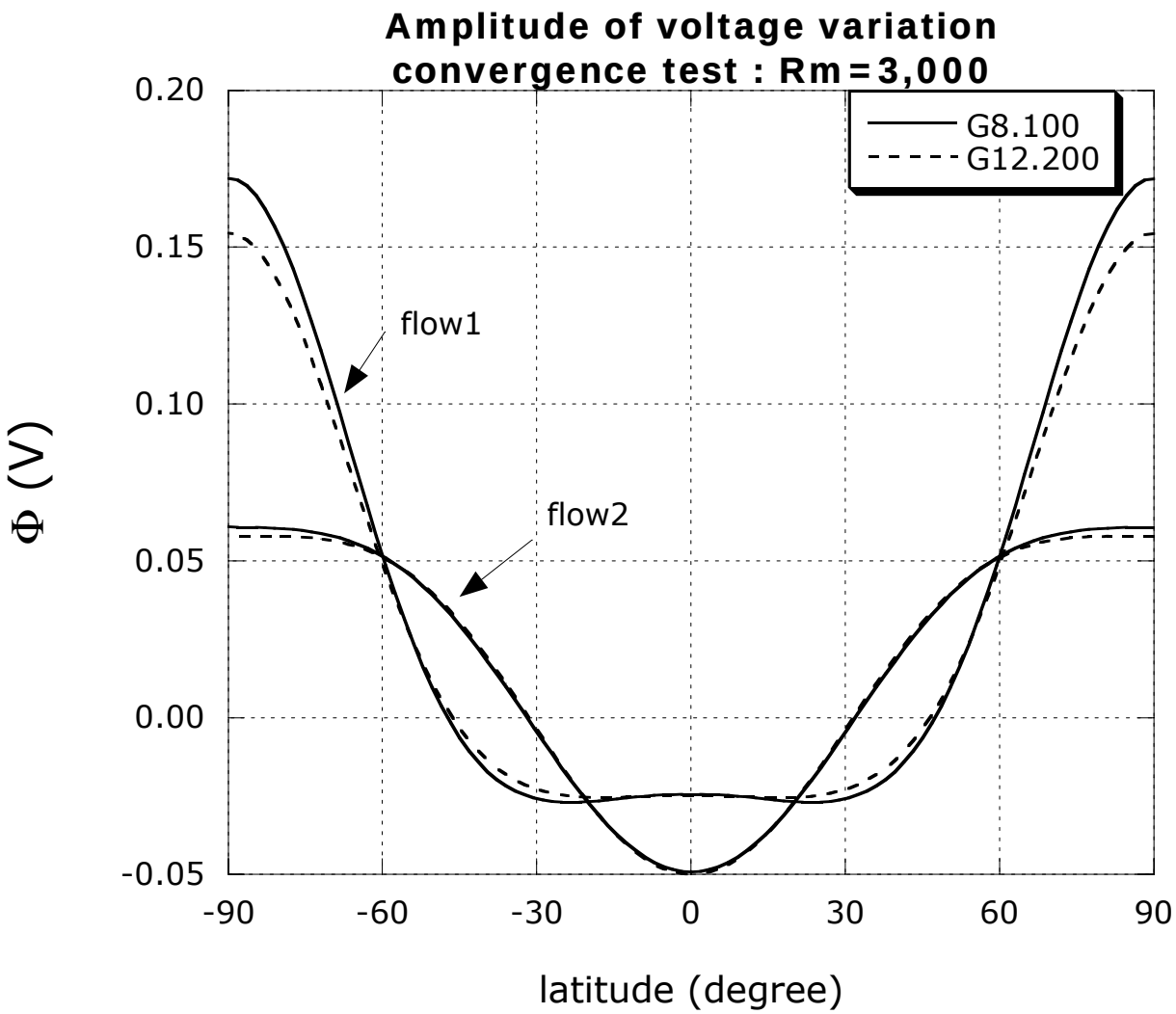
Amplitude of voltage variation
convergence test : Rm=3,000
G8.100
G12.200
flow1
flow2
Φ (V)
0.20
0.15
0.10
0.05
0.00
-0.05
-90
-60
-30
0
30
60
90
latitude (degree)

Figure B2